

Application of Silicon Photomultipliers to Positron Emission Tomography

EMILIE RONCALI¹ and SIMON R. CHERRY²

¹Department of Biomedical Engineering—GBSF 2603, University of California, Davis, One Shields Avenue, Davis, CA 95616, USA; and ²Department of Biomedical Engineering—GBSF 2511, University of California, Davis, One Shields Avenue, Davis, CA 95616, USA

(Received 4 October 2010; accepted 29 January 2011; published online 15 February 2011)

Associate Editor Angelique Louie oversaw the review of this article.

Abstract—Historically, positron emission tomography (PET) systems have been based on scintillation crystals coupled to photomultiplier tubes (PMTs). However, the limited quantum efficiency, bulkiness, and relatively high cost per unit surface area of PMTs, along with the growth of new applications for PET, offers opportunities for other photodetectors. Among these, small-animal scanners, hybrid PET/MRI systems, and incorporation of time-of-flight information are of particular interest and require low-cost, compact, fast, and magnetic field compatible photodetectors. With high quantum efficiency and compact structure, avalanche photodiodes (APDs) overcome several of the drawbacks of PMTs, but this is offset by degraded signal-to-noise and timing properties. Silicon photomultipliers (SiPMs) offer an alternative solution, combining many of the advantages of PMTs and APDs. They have high gain, excellent timing properties and are insensitive to magnetic fields. At the present time, SiPM technology is rapidly developing and therefore an investigation into optimal design and operating conditions is underway together with detailed characterization of SiPM-based PET detectors. Published data are extremely promising and show good energy and timing resolution, as well as the ability to decode small scintillator arrays. SiPMs clearly have the potential to be the photodetector of choice for some, or even perhaps most, PET systems.

Keywords—Silicon photomultipliers, Geiger-mode avalanche photodiodes, Positron emission tomography.

INTRODUCTION

Positron emission tomography (PET) involves injection of trace amounts of biomolecules labeled with a positron-emitting radionuclide and subsequent detection of the two back-to-back 511 keV photons produced simultaneously following positron–electron annihilation within the tissue. From the first development of

positron scanners^{12,73} and positron emission tomography (PET) systems in 1960s and 1970s^{67,98} to today's sophisticated commercial PET scanners, the vast majority of designs have been based on scintillation crystals coupled to photomultiplier tubes (PMTs). The 511 keV annihilation photons interact in the scintillator producing a short-duration pulse of visible light. The PMT converts these optical photons into electrons and multiplies them to create a detectable charge pulse that signifies the detection of an interaction. PMTs are very sensitive photodetectors combining high gain (amplification of signal by a factor of 10^6 to 10^7) with fast timing and are manufactured in a wide range of geometries and sizes. They represent a mature photodetector based on vacuum-tube technology that has been continuously improved over many years. Advances have included enhanced quantum efficiency,⁵³ improvements in timing performance, and multichannel and position-sensitive PMTs that allow localization of incoming scintillation photons on the photocathode. Nonetheless, their limitations in terms of quantum efficiency (fraction of incident light photons converted into electrons), bulky package size, and relatively high cost per unit surface area, along with the emergence and growth of new applications for PET that have quite demanding requirements, open opportunities for other photodetector designs. This review explores the potential of an emerging technology, silicon photomultipliers (SiPMs), as an alternative photodetector for PET applications.

Trends in PET Scanner Instrumentation

PET is widely used as a clinical and research tool for imaging cancer and a variety of neurological and cardiovascular disorders.^{4,21,56} Most scanners are designed for whole-body imaging, although some smaller dedicated devices for the brain and for breast cancer imaging have been developed. Systems are also available for preclinical imaging,⁴⁰ with a focus on

Address correspondence to Emilie Roncali, Department of Biomedical Engineering—GBSF 2603, University of California, Davis, One Shields Avenue, Davis, CA 95616, USA. Electronic mail: eroncali@ucdavis.edu

high-resolution imaging in rodent models of human disease and preclinical evaluation of new therapeutic approaches. PET scanners often consist of rings or arrays of detector modules that surround the subject, commonly in a cylindrical geometry.

For clinical systems, there is a desire to increase the axial length of the scanner, thus increasing the volume of tissue imaged at one time, and increasing solid angle coverage of the detectors with respect to the radionuclide emissions within the body. This can shorten imaging time, or allow reduction in the activity of the injected radiotracer reducing radiation exposure. However, it is offset by the roughly linear increase in cost (associated with more detector surface area) with increasing axial length. Lower cost photodetectors that can populate a large detector surface area would be desirable. A second trend is the incorporation of time-of-flight information, where the time difference of arrival of the two annihilation photons produced following the decay of a positron-emitting radionuclide, is measured.⁵⁹ This allows improved localization of an event and can improve signal-to-noise in the images. However, timing resolution for a pair of detectors must be significantly less than 1 ns for this to be effective. Time-of-flight PET therefore benefits from photodetectors that have a very fast pulse rise time such that the time an interaction occurs in the detector can be precisely determined.

The increasing role of preclinical imaging in the understanding of disease processes and the assessment of treatment efficacy has led to a rapid expansion of small-animal imaging in the last 20 years. The scale of the anatomical and functional features to be studied requires modified instrumentation, with enhanced spatial resolution and sensitivity,⁹⁶ where sensitivity is defined as the fraction of radioactive decays that results in a detected event within the scanner.

Sensitivity improvements can be achieved by reducing the ring diameter to match the size of the small-animal subject and achieve higher solid angle coverage. Approaches to obtaining high spatial resolution include the use of monolithic crystals combined with event localization algorithms^{46,54} or the use of arrays of small scintillator elements.⁹¹ In both cases, compact photodetectors that can be packed tightly around the subject are desirable to avoid sensitivity losses due to gaps between detectors. Furthermore, the best possible signal-to-noise is required to accurately define the location or crystal of interaction. In some proposed configurations, scintillation light is extracted from both ends of a scintillator array with one photodetector placed on each end.¹⁰⁴ This places even more stringent constraints on the physical size of the photodetector and the ability to pack them tightly together. Thus for preclinical PET applications, very

compact photodetectors that are capable of fine positioning are necessary. In addition, low cost is desirable for widespread adoption of such imaging systems in research laboratories.

Another trend has been to develop multimodal imaging systems combining anatomical and functional information, resulting in new clinical and research tools. The integration of PET and CT (X-ray computerized tomography) has been shown to improve diagnostic capability^{4,6} and all commercially available whole-body PET systems are now combined with CT. Preclinical scanners typically come with a CT component. Recently, the combination of PET with MRI (magnetic resonance imaging) has become a topic of interest, as such systems have great potential for soft tissue imaging⁸⁸ and whole-body imaging.¹⁶ In addition, simultaneous acquisition of both modalities enables the comparison and integration of various functional, physiologic, and metabolic parameters with the underlying anatomy and improves the accuracy of image registration. However, combining PET and MRI brings forth new technical challenges: in order to preserve the quality of the PET images, detectors must be insensitive to magnetic fields (field strengths in range of 1–12 T), and they must not degrade MR images by creating artifacts or decreasing signal-to-noise ratio. PMTs are extremely sensitive to magnetic fields and are therefore generally not suitable for PET/MRI. This application requires very compact and magnetic field insensitive photodetectors that can be packed in the confined bore of an MRI system. It would benefit from photodetectors that do not need supporting electronics (i.e., preamplifiers) to be placed close to the detector output where they would take up valuable space and increase the likelihood of interference with the MR system.

In each of these application areas, there is the potential for alternative photodetector technologies to play a role. PMTs, due to their combination of high gain, fast timing, and moderate cost, have shown remarkable longevity as the photodetector of choice for PET. However, in the silicon photomultiplier (SiPM), the topic of this review, has the PMT finally met its match?

Avalanche Photodiodes

Before discussing SiPMs, it is instructive to briefly consider the device upon which SiPMs are based, the avalanche photodiode (APD). APDs are compact silicon devices, based on a modified p–n junction structure, that overcome several of the drawbacks of photomultiplier tubes described above.⁸⁶ APDs are designed such that when a bias voltage is applied, a region with a very high electric field is created.

The field is high enough that charges produced in this region (e.g., by the absorption of light photons from a scintillator) may be accelerated sufficiently to create further electron-hole pairs in the region by impact ionization, thus causing a multiplication or “avalanche” of charges that are then collected to form an output pulse. The APD thus differs from a conventional photodiode in that it has internal gain. For PET applications, APDs are operated in proportional mode, just below the breakdown voltage. At this bias voltage, the gain is high, and the output signal is proportional to the amount of scintillation light interacting in the APD.

APDs exhibit very high quantum efficiency (up to 80 vs. 25% for PMTs) and are compatible with operation in high magnetic fields.⁸⁵ APDs have been incorporated in several small-animal PET scanners.^{5,105,107} APDs work with high bias voltages similar to those used with PMTs, however, they produce a much lower gain ($\sim 10^2$ to 10^3 as opposed to 10^6 to 10^7 for PMTs) and exhibit poorer timing resolution (APDs have a slower rise time than PMTs⁹⁷). Operating conditions for APDs are challenging, as they may require cooling to achieve adequate signal-to-noise, and careful temperature and bias voltage regulation is needed for stable operation, as the gain is a strong function of these two parameters. APDs have been available for several decades, and despite continuous improvements and successful incorporation in some PET systems, their overall performance characteristics and economics have not been sufficient to convince most manufacturers to replace their PMT-based designs.

Silicon Photomultipliers

SiPMs, also known as multi-pixel photon counters (MPPCs) or solid-state photomultipliers (SSPMs),¹ represent an alternative solution that to a large extent combines the advantages of PMTs and APDs. They have high gain (equal or greater than PMTs) are operated at moderate bias voltages (< 100 V).¹³ They are relatively insensitive to magnetic fields²⁹ and thus are a good candidate for PET/MRI applications. Like APDs, SiPMs require careful temperature control for stable operation because their gain is sensitive to temperature variations. However, many applications do not require preamplification or cooling to achieve adequate signal-to-noise levels. Excellent timing properties of SiPMs also make them promising for

time-of-flight PET imaging. Some companies predict large-scale, high-yield manufacturing of SiPMs, and consequently low-prices, although the ultimate cost of this technology may take some time to become clear and will depend, in part, on the demand for SiPMs for other applications outside of the nuclear medicine field.

SiPMs clearly have the potential to be a suitable photodetector for some or even perhaps most types of PET scanners, but do not yet represent a mature technology. Astonishing progress has been made over the past 5 years, with designs, performance improvements, and larger-area sensors. This in turn opens the door wider for the exploration and ultimate adoption of these photodetectors for existing and developing PET scanner designs and applications. Although this review focuses entirely on the interest in SiPMs for PET imaging, these devices are being adopted for a variety of other applications in particle physics and single photon counting.^{13,23}

A TECHNICAL AND HISTORICAL DESCRIPTION OF SILICON PHOTOMULTIPLIERS

A Brief History

Solid-state single photon detectors were initially investigated in 1960s, followed by avalanche photodiodes operated in Geiger-mode (G-APDs), also known as single photon avalanche photodiodes. In Geiger-mode, the devices are operated above the breakdown voltage, thus producing a large output pulse, even for the detection of a single optical photon. These are excellent detectors for very low light level optical applications, but not very useful for PET, as the output pulse amplitude is independent of the number of scintillation photons striking the device. In PET, the number of photons produced in the scintillator is proportional to the energy of the detected gamma photon. If the detector output is not proportional to the number of scintillation photons, then the energy of the gamma photon cannot be determined and the system cannot reject lower energy events that have undergone a Compton scatter interaction in the subject.

A breakthrough occurred with the development of miniaturized Geiger-mode APDs in the early 1990s with the creation of the Metal-Resistor-Semiconductor (MRS) structures.^{26,76,79} An MRS structure consists of a thin layer of metal on top of a highly resistive material (typically Si_xO_y), deposited on a semi-conductor. It now became possible to build a photodetector, the SiPM, from a 2-D array consisting of large numbers of tiny G-APD elements, usually referred to as microcells. As explained below, this overcomes the disadvantage of

¹SiPMs are called by several different names depending on the specific design and manufacturer and this can be confusing. In this review we will use the term SiPM to generically describe all such devices and will avoid the use of specific product names except where it relates to a specific piece of data or otherwise is relevant.

a single G-APD, as the amplitude of the output pulse of a SiPM is proportional (over some range of intensities) to the number of photons incident on the surface of the device. There are now several SiPM designs that are commercially available (e.g., SensL,⁸⁴ Zecotek Photonics Inc.,¹⁰⁶ CPTA,²⁰ STMicroelectronics,⁹³ Hamamatsu Photonics,²⁸ Amplification Technologies,¹ Photonique SA.⁶⁸). The different arrangements, and their properties, are summarized in.⁷⁴

Overview of SiPM Structure and Operation

A SiPM is composed of a 2-D array of small APDs (called cells or microcells) designed to operate in Geiger-mode.² One individual cell or G-APD consists of a p-n junction with dimensions typically ranging from 10 to 100 μm . A thin depletion layer ($\sim 0.7 \mu\text{m}$) is formed between the p+ and n+ layer, with an electric field of $\sim 3 \times 10^5 \text{ V/cm}$. The avalanche occurs in the presence of the high electric field, which can accelerate the charge carriers and generate the avalanche. Because the depletion layer is so thin, the bias voltage necessary to achieve this high electric field is only tens of volts. The cells are joined together on a common silicon substrate and are electrically decoupled by polysilicon strips (Fig. 1a). The output signal is read out through aluminum strips (Fig. 1b). The n⁻ guard rings around the cells ensure a uniform electric field by preventing premature edge breakdown.³²

Each cell responds independently when incident optical photons interact in that cell. Electron-hole pairs generated by these incident photons are able to trigger a Geiger discharge when the device is operated above the breakdown voltage.²² Before the discharge is quenched via a quenching circuit (Fig. 2a), each cell accumulates a charge Q_{cell} that is independent of the incident light:

$$Q_{\text{cell}} = C_{\text{cell}} \times (V_{\text{bias}} - V_{\text{breakdown}}) \quad (1)$$

C_{cell} is the capacitance of a cell, V_{bias} is the applied voltage, and $V_{\text{breakdown}}$ is the breakdown voltage for the G-APD cell. A typical value for the capacitance of a cell is 100 fF and the overvoltage ($V_{\text{bias}} - V_{\text{breakdown}}$) applied to the device is a few volts. The charge accumulated by a cell is therefore on the order of 200 fC, which results in a cell gain of about 10^6 .^{15,27} The readout of the array of cells within a SiPM is performed via a common load resistor. As individual cells operate

like binary devices, the output signal of the SiPM is proportional to the number of cells that fired.

When illuminated by a low-intensity light source (number of photons \ll number of microcells), assuming there is good gain uniformity between the cells, a SiPM produces output pulses with amplitudes proportional to the number of photons that are converted into a Geiger discharge within the device. This can be observed by acquiring a pulse height spectrum under low-intensity illumination. Figure 3 shows three normalized pulse height spectra acquired for a blue LED biased and pulsed to produce three different light levels. Peaks corresponding to the statistical fluctuations in the discrete number of photoelectrons generated for each detected pulse are clearly seen. Linearity and saturation effects will be discussed later.

In Geiger-mode, the avalanche will be self-sustaining and must therefore be quenched to reset the cell and make it ready to detect another photon. The output of each microcell is terminated by either passive or active quenching. Passive quenching of a cell is commonly obtained via a resistor placed in series with the G-APD whereas active quenching requires circuitry such as comparators to detect the presence of a photodetection and rapidly quench the avalanche and reset the cell.^{9,10,99}

In the initial state the device is charged at $V_{\text{bias}} > V_{\text{breakdown}}$. The response of a SiPM to incident light can be summarized in three simplified steps using the model in Fig. 2b:

1. Discharge: When optical photons hit a cell, a unit impulse of charge is produced independent of the number of incident photons and the capacitance C_{cell} discharges through R_{cell} . The output of the SiPM is proportional to the number of cells that fired.
2. Quenching: In passive quenching, the reverse voltage decreases to $V_{\text{breakdown}}$ when current flows through the quenching resistor placed in series (Fig. 2b) with the cell. The avalanche process stops.
3. Recharge: The voltage returns to V_{bias} .

PROPERTIES OF SILICON PHOTOMULTIPLIERS

To characterize a photodetector and its ability to perform the task it will be assigned, three important criteria should be considered: (1) the signal-to-noise ratio with respect to the level of signals to be detected, (2) the dynamic range, and (3) the timing properties with respect to the time scale of the signals of interest. These performance criteria are determined by the

²A fundamental difference between a Geiger mode APD compared to a proportional APD is that it is reversed biased above the breakdown voltage. This allows the generated carriers to trigger avalanche multiplication, resulting in a self-sustaining breakdown. These devices require a quenching circuit to terminate the avalanche process.

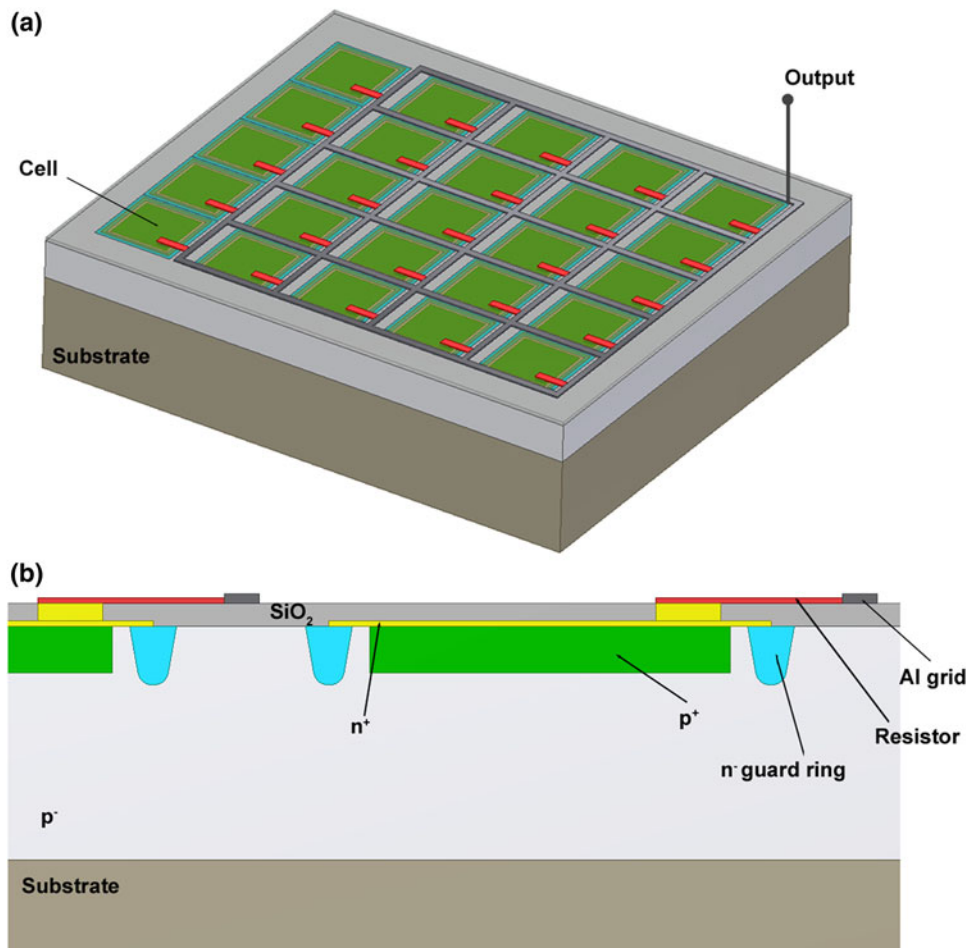


FIGURE 1. (a) Simplified structure of a SiPM composed of G-APD cells. The G-APDs are joined together on a common substrate and are electrically decoupled. The outputs of the cells are connected to an Al grid used for the readout of the output signals. Each cell has a quenching resistor in series. (b) Each cell (G-APD) is a p-n junction with a very thin depletion layer between p+ and n+ layers.¹⁵ Drawings courtesy of Julien Bec, UC Davis.

properties of the individual G-APD cells, as well as the number of cells and their geometry within the SiPM, and have been described extensively.^{7,8,15,22,44,49,92}

For a given incident light level, the signal produced by a silicon photomultiplier depends primarily on the gain and the photodetection efficiency (PDE), where the PDE is defined as the fraction of incident photons that lead to a Geiger discharge and therefore a detectable signal. The major noise source arises from thermally generated pulses. We briefly examine each of these properties.

Gain

The gain of a SiPM cell depends on the charge accumulated by a cell (Eq. 1) and typically ranges between 10^5 and 10^7 , depending on the bias voltage and the temperature (Fig. 4a). The gain is quite sensitive to bias voltage and the temperature at a given bias voltage. Gain drifts of up to $5\%/^{\circ}\text{C}$ have been

observed: $2.7\%/^{\circ}\text{C}$ for $3 \times 3 \text{ mm}^2$ SiPM (Photonique SA) and $5\%/^{\circ}\text{C}$ for $3 \times 3 \text{ mm}^2$ multi-pixel photon counters (MPPC, Hamamatsu Photonics) by Kolb *et al.*³⁶ The primary reason that the gain changes with temperature in a SiPM is that the breakdown voltage varies with temperature. A linear increase in breakdown voltage of a few tens of $\text{mV}/^{\circ}\text{C}$ is generally observed;^{49,92} if the bias voltage is kept constant as the temperature increases, the overvoltage (difference between the bias voltage and the breakdown voltage) decreases. The gain plotted as a function of overvoltage is constant with temperature (Fig. 4b), demonstrating that the temperature effect is explained in large part by the change in breakdown voltage.⁷²

Photodetection Efficiency (PDE)

In principle, a SiPM can produce a detectable pulse from the interaction of a single optical photon. In practice, however, not all incident photons lead to a

Geiger discharge in the device, and thus the efficiency with which photons are converted to a signal, the photodetection efficiency (PDE), is significantly less than 100% (Fig. 5). The PDE is defined as the product of three terms: the fill factor FF (ratio of the active area of the microcells to the total area of the SiPM), the probability of Geiger discharge P_g , and the quantum efficiency QE:

$$\text{PDE} = \text{FF} \times P_g \times \text{QE} \quad (2)$$

The fill factor is a constant parameter inherent to the geometry of the device. The microcells are surrounded by a dead area, which makes the cell pitch a few microns larger than the size of the cell itself. Typical fill factors in current devices are in the range of 20–80%.^{28,71,84}

Not all electron-hole pairs produced necessarily lead to a Geiger discharge, depending on where in the device they are produced and the likelihood of competing processes such as recombination. The Geiger discharge probability accounts for this, and is a function of the probability that holes and electrons trigger a discharge. This factor depends on the location of the primary electron-hole pair and the electric field shape, and increases with overvoltage.⁶⁵ Typical values for P_g are 0.5–1.⁷⁰

The quantum efficiency is strongly wavelength dependent and depends on temperature. This is reflected in the PDE curves shown in Figs. 5a and 5b.

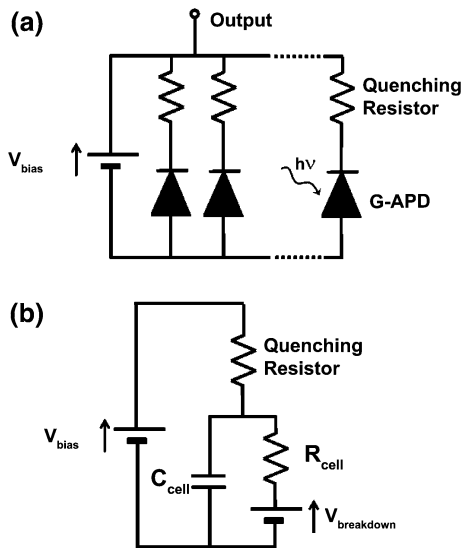


FIGURE 2. (a) Simplified electric structure of a SiPM composed of several G-APDs in series with a quenching resistor. (b) Equivalent circuit of a single cell when the device is on (a bias voltage V_{bias} is applied) and is detecting photons. The capacitor C_{cell} initially charged at V_{bias} discharges through R_{cell} dropping the bias voltage to $V_{\text{breakdown}}$. The avalanche process is quenched via the quenching resistor and then the device is recharged.

The quantum efficiency of silicon is greater than 80% over the visible range, but the absorption in silicon (absorption length is $1 \mu\text{m}$ at 450 nm; $5 \mu\text{m}$ at 650 nm) limits the detection of blue photons to shallow layers. For this reason, G-APDs dedicated to detection of blue light are generally based on a shallow junction design with the junction located at a depth of $0.5 \mu\text{m}$ or less.

Two types of structures are used in SiPMs: p-on-n or n-on-p configurations. When the first layer is a p layer (p-on-n structure), shorter wavelength (blue) photons will tend to interact in that layer producing electrons that move towards the junction under the influence of the electric field. Since electrons have a higher chance to trigger an avalanche breakdown than holes, the Geiger probability is optimized. Conversely, longer wavelength (red) photons travel further into the material and will tend to be absorbed by the n layers, and the resulting holes will drift towards the junction. The Geiger probability is then reduced. p-on-n structures thus exhibit a higher PDE at shorter wavelengths. In the case of n-on-p structures, the situation is reversed and the shorter wavelength photons will tend to trigger the avalanche via holes with a lower probability of Geiger discharge, while the longer wavelength photons will start the avalanche with electrons. Hence, this latter type of structure has a lower PDE in the blue and must be operated at higher overvoltage to provide reasonable sensitivity in this spectral region.

For applications in PET, a higher sensitivity in the blue region is desirable, as the emission spectra of common PET scintillators peak in this part of the spectrum (Fig. 6).^{35,52} Therefore, structures with a good sensitivity in the blue region such as p-on-n, or

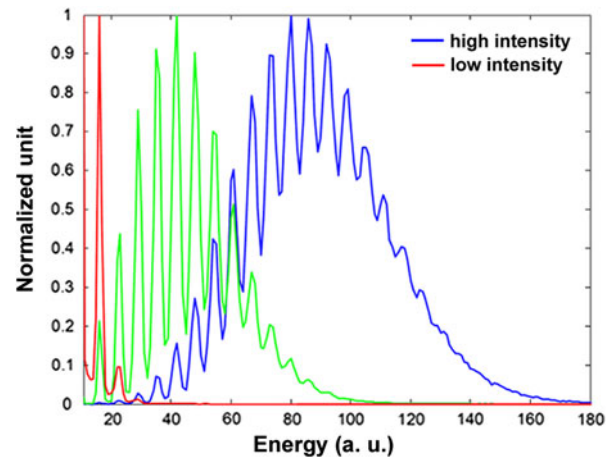


FIGURE 3. Pulse height spectra from a $1 \times 1 \text{ mm}^2$ Hamamatsu MPPC S10362-11-025C acquired for three different light intensities (the red and blue curves correspond to the lowest and strongest intensities, respectively) showing peaks corresponding to different numbers of photoelectrons generated.

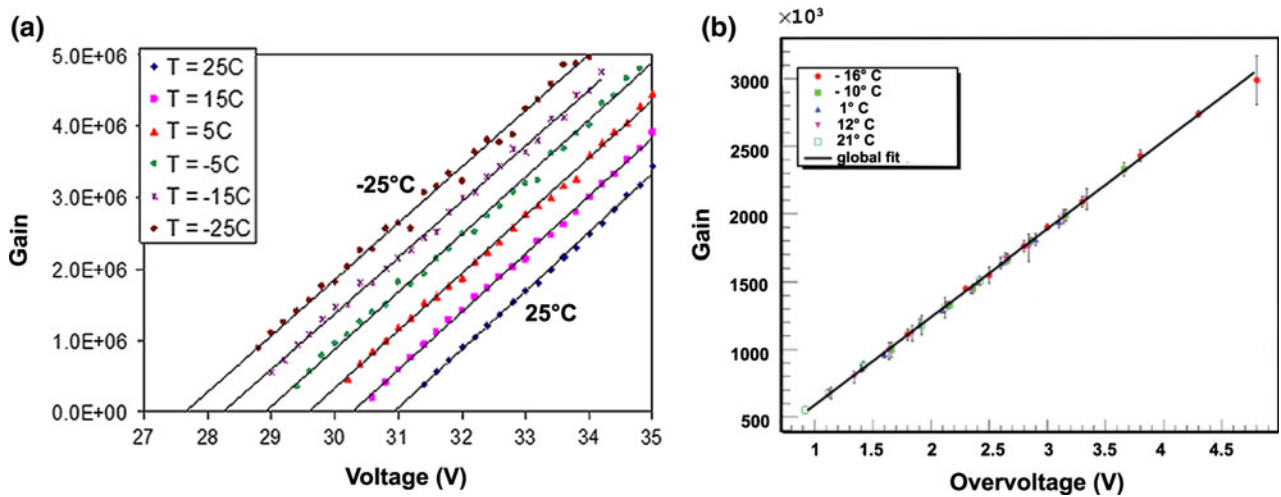


FIGURE 4. (a) Variation of gain as a function of bias voltage for a $1 \times 1 \text{ mm}^2$ SiPM with 400 cells, at different temperatures (from left to right: -25 , -15 , -5 , 5 , 15 , and 25 °C) Piemonte *et al.*⁷¹ © 2008 IEEE. (b) Gain as a function of overvoltage for different temperatures for a $1 \times 1 \text{ mm}^2$ SensL SPM. Ramilli⁷² © 2008 IEEE.

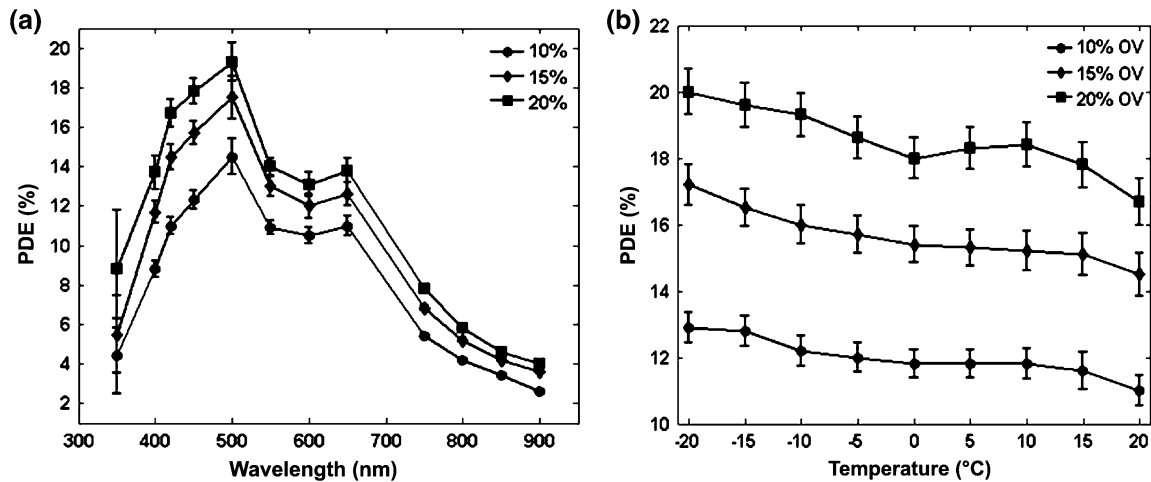


FIGURE 5. (a) PDE spectra for different overvoltages (10, 15, and 20%) acquired with a $1 \times 1 \text{ mm}^2$ SiPM (STMicroelectronics) with 289 cells and a fill factor of 48%. Mazillo *et al.*⁴⁹ © 2009 IEEE. (b) PDE as a function of temperature for different overvoltages (10, 15, and 20%) for the same device as (a). Mazillo *et al.*⁴⁹ © 2009 IEEE.

specifically designed n-on-p structures for enhanced detection of blue light (discussed later), are preferable.

The reported photodetection efficiency varies over a wide range, depending on the G-APD design, the overvoltage and whether confounding factors such as afterpulsing and optical crosstalk (discussed in next section) are included. Values reported in literature at 420 nm range from about 5 to 50%,^{44,92} however, comparisons must be made with care due to the strong dependence of the values on the exact methodology used for the measurement.

Sources of Noise and Spurious Pulses

In SiPMs the main source of noise is thermally generated. The high gain of SiPMs makes the

electronic noise negligible with respect to this thermal noise,⁸ a very different situation compared to avalanche photodiodes that have a much lower gain (10^2 to 10^3). Thermal noise, characterized by the dark count rate (number of pulses per second with no light source), arises from charge carriers created in the sensitive area of the device, which can trigger an avalanche in the presence of high electric field. The dark count rate increases with the area of the device, temperature, and overvoltage.^{7,92} It ranges from around 1 MHz/mm² at room temperature to a few kHz/mm² at -20 °C. Most dark noise pulses have an amplitude of 1 photoelectron. The probability of higher amplitude pulses arising from several simultaneously generated charge carriers drops by roughly an order of magnitude for each additional photoelectron.²³

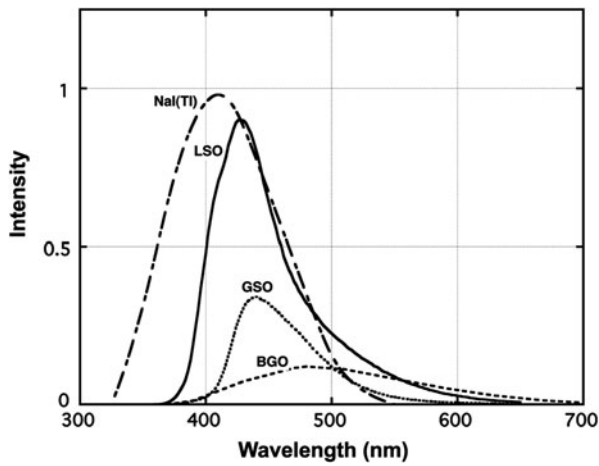


FIGURE 6. Emission spectra for scintillators commonly used in PET: sodium iodide (NaI(Tl)), lutetium oxyorthosilicate (LSO), gadolinium silicate (GSO), bismuth germanate (BGO). Melcher *et al.*⁵² © 1992 IEEE.

In PET, the optical photon fluence from the scintillator is generally high and short integration times are used. These dark pulses can be virtually eliminated by setting a pulse height threshold at the level of a few photoelectrons, which is well below the average light level produced by the interaction of a 511 keV photon in a scintillator. Therefore, for many detector designs, the thermal noise from the SiPMs is not a limiting factor.⁶⁶ However, for designs that determine position based on an accurate measure of the light-spread function,^{47,54,80} or configurations that involve multiplexing of signals across many SiPMs, thermal noise may degrade performance.

Two other phenomena can lead to spurious pulses in a SiPM: optical crosstalk between cells and the afterpulsing. Optical photons can be produced within a G-APD cell operated at the breakdown voltage (3×10^{-5} photons per electron crossing the junction^{39,62}) and can potentially move to a neighboring cell and trigger an avalanche breakdown just as an incident photon would. This phenomenon is called optical crosstalk and varies between 1 and 50% for different structures and different overvoltages.^{14,27,72,92}

The optical crosstalk generates output pulses indistinguishable from true signals and can result in two cells within a SiPM firing even though only 1 photon was detected. If not corrected for, optical crosstalk can result in an overestimation of the PDE. To reduce crosstalk, cells need to be optically isolated. Current solutions include using a larger pitch between cells, or creating trenches filled with an opaque material between the cells.^{32,49,70} Both these solutions, however, reduce fill factor and adversely effect the PDE. Afterpulsing occurs when a charge carrier is trapped during a Geiger discharge and released after a certain

delay to trigger a new avalanche. The incidence varies with overvoltage between 0.3 and 10%^{24,92} and increases when the temperature decreases because of a longer trapping time. Afterpulsing depends on the cell recovery time (thus on the quenching circuit).¹⁴ Afterpulsing can lead to a single scintillation event producing two pulses and can be a confounding factor in PDE measurements.

Dynamic Range and Linearity

The dynamic range must be considered with respect to the range of signal amplitudes to be measured. Low photon fluence requires high sensitivity whereas high photon fluence detection, such as that produced by scintillators used in PET detectors (thousands of optical photons per 511 keV annihilation photon interaction), necessitates a large dynamic range. As previously discussed, the output signal of a SiPM is the sum of the signals of the firing cells, and is therefore correlated to the number of incident photons. The dynamic range is determined by the number of cells in the device, and linearity of the SiPM signal with light intensity is only maintained as long as no more than one optical photon interacts per SiPM cell (illustrated in Fig. 7a). At higher light intensities where this condition is violated, there will be saturation of the signal leading to non-linearity with the incident light levels. In the case of PET, this will result in a non-linearity between the detector signal and the energy deposited in the scintillator, thus degrading the ability to reject Compton-scattered annihilation photons based on their energy loss, or to reject pulse pile-up due to two annihilation photons interacting in the same scintillator element at the same time. The relationship between the number of firing cells (N_{fired}), the number of optical photons incident on the device (N_{phot}) and the number of microcells in the device (N_{cells}) can be approximated by⁹² (Fig. 7b):

$$N_{\text{fired}} = N_{\text{cells}} \left(1 - \exp \left(-\text{PDE} \times \frac{N_{\text{phot}}}{N_{\text{cells}}} \right) \right) \quad (3)$$

The detector response is linear if the term $\text{PDE} \times N_{\text{phot}}/N_{\text{cells}}$ is rather small. For a device of a given area, a large number of cells would be preferred for PET applications as a few thousands of photons can be expected to reach the surface of the SiPM. For example, a 511 keV annihilation photon interacting via the photoelectric effect in lutetium oxyorthosilicate (LSO) scintillator produces ~12,500 optical photons. However, increasing the number of cells in a given area requires reducing the size of the cells, and this typically reduces fill factor and thus PDE. There is therefore a trade-off between dynamic range and detection efficiency.

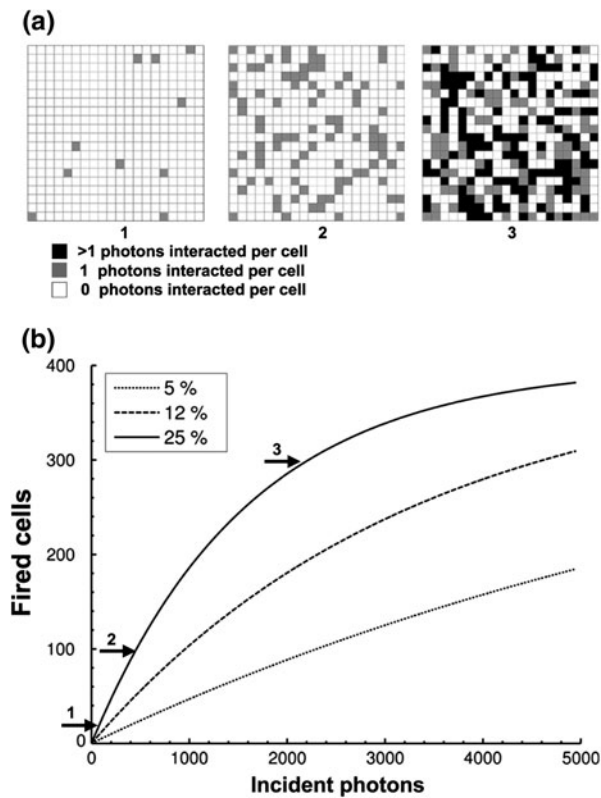


FIGURE 7. (a) Representation of a 400-cell SiPM at different light levels that results in (from left to right) 10, 100 and 300 cells firing. The grey scale indicates the number of photons interacting per cell and was calculated from Eq. (3), for a PDE of 25%. (b) Number of fired cells vs. number of incident photons: illustration of Eq. (3) for a SiPM with 400 cells and different PDE values (5, 12, and 25%).

Timing Properties

The timing properties of SiPMs are controlled by the Geiger discharge time and the recovery time. These two parameters define the shape of the output signal by controlling its rise time and decay time. The Geiger discharge is generally fast (\sim a few hundred ps). The rise time of the output signal is typically a few ns. The decay time depends on the recovery time thus on the quenching circuit: for a passive quenching the time constant given by the product of $R_{\text{cell}} \times C_{\text{cell}}$ is usually about 30 ns¹⁵ or shorter. Both the rise time and decay time increase with the total capacitance of the SiPM. The capacitance of the photodetector increases with its area with typical values being 30 pF for a 1 mm² SiPM and 320 pF for 9 mm² SiPM.²⁸ Devices with larger areas will therefore be slower. In a scintillation detector, the measured output pulse also is a function of the scintillator rise and decay times.

The statistical variation in the response time of the device to an incident optical pulse, due to the time jitter of the cells, determines the timing resolution. Time

jitter is caused by fluctuations in the Geiger discharge time and by the statistical variation of the detection time of the incident photons due to the decay characteristics of the scintillator. The Geiger discharge time varies with the location of the generated charge carriers.⁹² The time jitter is usually between 60 and 100 ps,^{24,44,92} thus excellent timing resolution is theoretically possible with SiPMs.

ADVANCES IN DESIGN, PERFORMANCE, AND MANUFACTURING

From the perspective of integrating silicon photomultipliers in PET detectors, the technology still has room for improvements. First, the light intensities obtained from scintillation crystals are strong enough to necessitate a wide dynamic range, which requires a large number of cells in the sensitive area. This gets particularly challenging for small scintillator crystals used for high-resolution PET applications as the light intensity per mm² can be quite high and it is difficult to get high fill factors (while minimizing optical cross-talk) when the cells are extremely small. Secondly, PET scanners generally incorporate detector blocks or modules that range in surface area from 20 × 20 mm² to 40 × 40 mm² and where individual crystal identification is multiplexed for cost considerations and to reduce the number of electronic channels. As an example, LSO-APD block detectors with a total area of 20 × 20 mm² (10 × 10 LSO array with a crystal size of 2 × 2 × 12 mm³ coupled to 3 × 3 arrays of 5 × 5 mm² APDs) have been developed for high-resolution PET.⁶⁹ Such a design would require SiPMs with dimensions larger than those currently available. For clinical detectors, even larger-area devices approaching 10–20 mm in size might be desirable. Lastly, building complete PET scanners based on SiPMs will pose the challenge of producing thousands of silicon photomultipliers with uniform properties and that operate robustly for many years under bias at reasonable manufacturing cost.

As the issues of device area and dynamic range are addressed, there are several competing factors that must be considered. Larger-area devices will result in a higher dark count rate. For a given device area, decreasing the size and increasing the number of cells will increase dynamic range, but will reduce the PDE by adversely affecting the fill factor. Hence, to maintain a reasonable PDE it is critical to have an optimized structure, with enhanced detection of blue light for PET detectors, and to maximize the Geiger discharge probability.

Although p-on-n structures are intrinsically favorable to the readout of scintillation crystals whose

emission is mainly in the blue part of the spectrum, high PDE may be obtained by enhanced n-on-p structures. Several designs, based on MRS structures, have been proposed by Sadygov *et al.*⁷⁷ A buried junction configuration with the p–n junction located $\sim 0.8 \mu\text{m}$ below the surface, with a depletion layer less than $1 \mu\text{m}$ thick was investigated by Piemonte *et al.*⁷⁰ Such a configuration maximizes the triggering probability (Geiger discharge always triggered by electrons) and the fill factor. Moreover, antireflective coating such as silicon oxide and silicon nitride can be applied on the top layer to increase the sensitivity in the blue and near ultraviolet⁴⁹ by decreasing the reflectance of the first layer.

Quenching resistors are usually made of highly resistive polysilicon, which is a strong absorber of light. SiPMs with bulk integrated quenching resistors avoid the use of polysilicon and can potentially lead to a higher PDE.⁶³ In addition, this approach has an excellent packing fraction. However, even though the fill factor is usually limited by layout considerations, connections,⁴⁵ and fabrication, a dead space between cells must be maintained in order to limit optical crosstalk. A reasonable trench width is $\sim 4 \mu\text{m}$, which leads to only a 36% fill factor for $30 \mu\text{m} \times 30 \mu\text{m}$ cells.⁷⁰

Since larger-area devices are needed for PET, a higher fill factor and an improvement in PDE can be obtained by enlarging the total sensitive area, and increasing the cell size. However, this may pose dynamic range issues as the scintillation light for a given crystal dimension is now spread over fewer cells. Larger cells result in higher cell capacitance thus in a greater cell gain (Eq. 1), but also in a higher likelihood of dark counts. Finally, a higher gain will increase the number of secondary photons created in the junction and will therefore increase the optical crosstalk. Working at higher gain without suffering trade-offs in performance will require an improvement in dark count rate and reduction of optical crosstalk.

Improvements in cell density can be made with innovative structures such as the buried junction described above, or a design known as micropixel APDs (MAPDs). These MAPDs are based on a common p–n junction on a n-type substrate, with microwells.² This design⁷⁷ allows the production of high cell density SiPMs ($3 \times 3 \text{ mm}^2$ devices with 15,000–40,000 cells per mm^2).

SiPM Arrays and Position-Sensitive Devices

The size of commercially available SiPMs is currently limited to $\sim 10 \text{ mm}^2$ (in comparison, the size of APDs goes up to over 400 mm^2), although some devices under development are now in the $20\text{--}30 \text{ mm}^2$

range. The restricted device area is dictated both by manufacturing and noise considerations. One solution to overcome this limitation is to build SiPM arrays.

Earliest arrays consisted of discrete single element SiPMs packaged into small arrays.³⁶ Monolithic SiPM arrays are under active development^{70,108} and early devices are now commercially available. However, some manufacturing and operating challenges need to be considered. Current fabrication techniques do not guarantee an array in which the individual SiPMs have identical performance, especially when a large number of SiPMs in the array is desired. Breakdown voltage and gain can vary from one SiPM pixel to another, and some pixels can be non-functional. From the perspective of improving the yield when fabricating large-area SiPM arrays, identification of cells exhibiting early breakdown and non-functional devices should be carried out. This can be done through on-wafer characterization based on an automatic measurement of the current voltage characteristics in forward and reverse bias voltage mode, allowing the quenching resistance of each SiPM and dark current to be determined.

Various arrays have been produced with reasonable uniformity of breakdown voltage, quenching resistance, and dark current¹⁰⁸: 2×2 arrays of $4 \times 4 \text{ mm}^2$ SiPMs (total size $7.9 \times 8.1 \text{ mm}^2$) and 8×8 arrays of elements with a pitch of $1.5 \times 1.5 \text{ mm}^2$. Working with arrays (either arrays composed of SiPMs tiled together or monolithic arrays) raises practical issues such as a larger number of output readouts. Multiplexing of the electronic channels can be achieved using a resistive network readout (Fig. 8a), providing position information using Anger logic with the following formula:

$$X = \frac{(A + B) - (C + D)}{A + B + C + D}, Y = \frac{(A + D) - (B + C)}{A + B + C + D} \quad (4)$$

X and Y are the computed coordinates of where the light strikes the SiPM array, based on the four signal outputs from the corners of the resistive network (Fig. 8a). When coupled to an array of scintillator crystals (which need not necessarily match the pitch of the SiPM pixels), and by building a 2D histogram of the (X, Y) locations for a large number of scintillation events, one can build a crystal map where individual crystals in the array may be resolved (Fig. 8b). The smallest size crystal that can be resolved with this technique is a complex function of scintillator light output geometry, reflectors, and surface treatments, SiPM element size, gain, and dynamic range, and the effects of the resistive network on the SiPM signals.

SiPMs and arrays of SiPMs can be equipped with position-sensitive circuitry, such as a micro-resistor network between the microcells, thus giving position information at the microcell level, similar to the readout

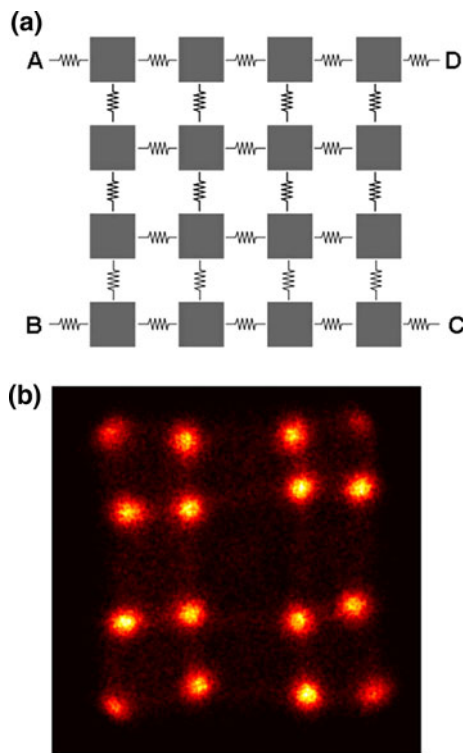


FIGURE 8. (a) Resistive network for a 4×4 SiPM array. (b) Crystal map acquired with a ^{22}Na source irradiating a 4×4 array of $1.5 \times 1.5 \times 20 \text{ mm}^3$ LSO scintillator crystals coupled to the SiPM array shown in Fig. 10a.

scheme described in Fig. 8. This technique has been applied to produce continuous PS-SiPMs (position-sensitive SiPMs) with a sensitive area as large as $5 \times 5 \text{ mm}^2$.^{50,51}

Integrated Circuitry and Digital SiPMs

To be a valid candidate for the next generation of PET scanners, the cost of large-area SiPMs or SiPM arrays has to be lowered, which requires designs that can be fabricated with standard processes (e.g., CMOS), and high manufacturing throughput and yield. For example, CMOS processes have the potential to allow low-cost SiPM fabrication with on-chip integrated electronics, such as pixel-level conditioning,¹⁸ position-decoding capability, or integrated quenching resistors.⁴⁸

This type of fabrication also allows the development of digital SiPMs.²⁵ In such a detector, each detected photon is converted to a digital signal that contains information on the number of microcells that fired and an associated timestamp. These devices are therefore intrinsically very fast²⁵ and active quenching built into each cell provides a short recovery time. Each cell is equipped with a static memory that allows the cell to be enabled or disabled. In this manner, cells with an

excessive dark current rate, for instance, could be switched off.

SILICON PHOTOMULTIPLIERS IN PET DETECTORS

The high gain, high photodetection efficiency, compact geometry and magnetic field insensitivity make SiPMs an attractive photosensor for the readout of scintillation crystals used in PET. Given the small area of current SiPM devices, much of the focus to date has been on decoding scintillator arrays with small elements designed for high-resolution PET applications such as small-animal or breast imaging. Due to the variability of SiPM properties with changes in temperature and overvoltage, an extensive characterization of SiPM-based PET detectors (crystal identification, energy resolution, and timing resolution) is needed together with an investigation of optimized operating conditions.

Energy Resolution and Dynamic Range

As the amplitude of a light pulse generated when an annihilation photon interacts with the scintillator crystal (via the photoelectric effect or Compton scattering) is proportional (ignoring slight non-linearities in the scintillation material itself) to the energy deposited in the crystal, the energy resolution of the detector will depend on the performance of the photodetector. In the case of SiPMs, the parameters of importance are the PDE which determines what fraction of the incident scintillation light photons are converted into Geiger-discharges, and the dynamic range, which if not sufficient can lead to non-linearities and distortions in the relationship between energy deposited and SiPM output.

Published data with $1 \times 1 \text{ mm}^2$ SiPMs coupled to LYSO or LSO crystals show that with a cell density of between 550 and 1000 per mm^2 , an energy resolution between 20 and 25% full width at half maximum (FWHM) can be achieved at 511 keV with non-optimized light collection.^{42,44,66,92} The dynamic range of a SiPM is determined by the number of cells in the device and by the number of available cells when incident photons interact with the SiPM. The number of available cells depends on the recovery time of the cells and can become an issue at higher counting rates. Energy resolution as good as $\sim 13\%$ has been measured with larger size SiPMs (with more cells and better dynamic range) of $1.5 \times 1.5 \text{ mm}^2$ to $5 \times 5 \text{ mm}^2$ (Fig. 9a) coupled to LSO or LYSO crystals.^{36,51,61}

In general, energy resolution improves with better PDE. Therefore, one may conclude that a higher

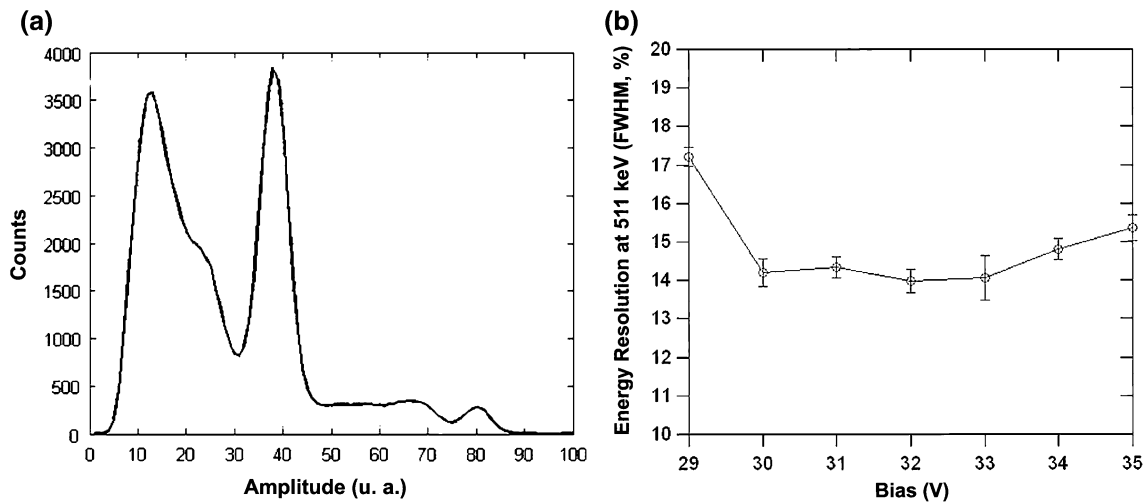


FIGURE 9. (a) ^{22}Na pulse height spectrum acquired at 23 °C with a $2 \times 2 \times 10 \text{ mm}^3$ polished LSO crystal coupled to a $5 \times 5 \text{ mm}^2$ PS-SiPM (RMD Inc). Data courtesy of Jeffrey Schmall, UC Davis. (b) Energy resolution vs. bias voltage for a $5 \times 5 \text{ mm}^2$ PS-SiPM (RMD Inc) coupled to a $5 \times 5 \times 3 \text{ mm}^3$ LSO crystal. McClish *et al.*⁵¹

overvoltage (which increases the Geiger probability and thus PDE) will give better results. However, the overvoltage increases the dark count rate and optical cross-talk. Therefore, there is only a narrow bias range, typically, several tenths of a volt, where the energy resolution is optimized (Fig. 9b). Since the overvoltage varies with temperature, this indicates that the energy resolution will be dependent on the temperature.

The measured energy resolution is also affected by the cell density. Non-linearities in SiPM signal with increasing energy (and therefore light level) are observed (Fig. 10) due to the finite number of cells in the SiPM. This non-linearity typically degrades the energy resolution and downshifts the photopeak position,^{36,61} and should be corrected when one wants to assess the energy resolution.⁴⁵ The energy spectrum can be corrected by linearization of the amplitude scale using a calibration curve (plot of SiPM response as a function of energy).⁶¹ In extreme cases where the scintillation light levels exceed the number of cells, the energy resolution becomes meaningless as all events cause all cells to fire and the SiPM output no longer depends on energy.

Although LSO and LYSO are currently the most popular scintillation crystals for PET, some other scintillator materials, such as LuYAP, are of interest^{60,78} and have been tested with SiPMs. LuYAP has a light yield of $\sim 12,000$ photons per MeV and a peak emission at 380 nm. An energy resolution of 25% was measured with $2.1 \times 2.1 \text{ mm}^2$ SiPMs (1764 microcells, PDE of 29% measured at 420 nm) coupled to a LuYAP crystal. This is worse than the 13% measured with the same SiPM with LSO and can be explained by the lower light yield of LuYAP and the lower quantum efficiency of the SiPM at 380 nm.⁶¹ LaBr_3 scintillator crystals are attractive for time-of-flight PET as they

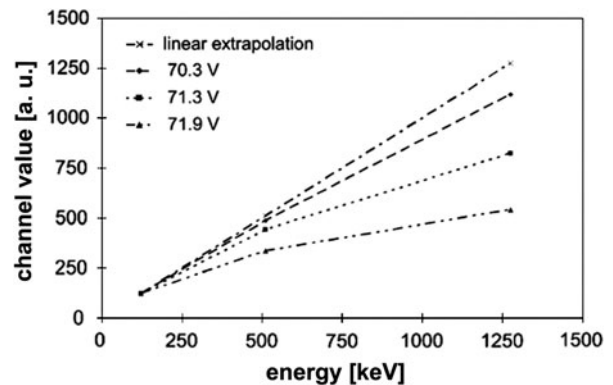


FIGURE 10. SiPM response as a function of energy for different bias voltages. Values are normalized to the response at 122 keV (^{57}Co).³⁶ Data were acquired with a $1 \times 1 \text{ mm}^2$ SiPM with 3600 cells. Non-linearity worsens with increasing bias voltage, as for a given incident light level, more cells fire (increased Geiger discharge probability) and saturation occurs earlier.

have a fast decay time ($< 25 \text{ ns}$) and a high light yield (70,000 photons/MeV, peak wavelength 380 nm).^{37,87} $\text{LaBr}_3\text{:Ce}$ (5%) crystals with a size of $3 \times 3 \times 5 \text{ mm}^3$ were tested with $3 \times 3 \text{ mm}^2$ SiPMs (3600 microcells, PDE 45% at 380 nm, including crosstalk and after-pulsing effects). An excellent energy resolution of $\sim 3.5\%$ at 511 keV was measured with a ^{22}Na source.⁸²

Decoding Scintillator Crystal Arrays

To decode arrays of scintillator crystals for imaging by PET, it is necessary to use either an array of SiPM elements (either individual elements packaged together or a true monolithic array) or SiPMs with position-sensing capability. In both cases, as discussed earlier, position information is typically obtained using

some form of charge-sharing or resistive circuit between the elements to multiplex the readouts and reduce the number of electronic channels needed. This is the same form of multiplexing employed in conventional PET detectors based on PMTs. More recently, application specific integrated circuits (ASICs) have been developed enabling the readout of many SiPMs (up to 64).^{19,75}

When working with arrays of SiPMs the homogeneity of each device becomes very important, as gain non-uniformity can cause degradation of the overall detector performance and distortions in position information. Feasibility of position-sensitive SiPM arrays has been demonstrated with 2×2 and 4×4 arrays of $1 \times 1 \text{ mm}^2$ SiPMs.^{44,45} These devices show a good pixel gain uniformity (4% variation in gain), noise uniformity, photopeak position (4.4% variation) and good uniformity in energy resolution: $15 \pm 3.2\%$ FWHM was measured at an overvoltage of 4 V. These SiPM arrays showed reasonable position determination when coupled to continuous scintillator crystals.⁴⁵

A custom-made 3×3 array built from 9 single-channel SiPMs with a 3.5 mm interpixel gap, coupled to an 12×12 element LSO array³⁶ showed good uniformity in energy resolution: 19.3% in the center crystals to 22% in the edge crystals. This variation is comparable to what can be expected from LSO-APD based detectors.¹⁰⁴ In addition, all the 144 crystals (individual size $1.5 \times 1.5 \times 20 \text{ mm}^3$) could be resolved in the crystal map. $5 \times 5 \text{ mm}^2$ position-sensitive SiPMs (Fig. 11a) have shown the ability to resolve $0.5 \times 0.5 \times 5 \text{ mm}^3$ individual crystals in an LSO array (Fig. 11b).⁵¹ These data show that multi-element or position-sensitive SiPM devices can resolve the size of scintillator elements being used for even the most demanding high-resolution PET applications.

Depth-Encoding PET Detectors

PET scanners, especially those employing high-resolution detectors and designed with small ring

diameters for brain, breast and small-animal imaging, are prone to non-uniform spatial resolution across the field of view due to parallax errors. The spatial resolution degrades rapidly with distance from the center of the transverse field of view.⁵⁷ To avoid this degradation, depth of interaction (DOI) information must be incorporated into the detector, such that the detector reports not just which scintillator element an annihilation photon interacted in, but also the depth at which it interacted in that element. Various depth-encoding detector designs have been proposed (Fig. 12a). For example, pulse shape discrimination (PSD) methods have been used with combinations of crystal layers with different decay times and provide discrete DOI information with a resolution of $\sim 5 \text{ mm}$ ^{64,83} defined by the thickness of the different crystal layers. Continuous DOI information with a resolution of 2–3 mm can be achieved with dual-ended read out of the scintillator arrays by position-sensitive APDs.¹⁰⁵ Several groups have now measured similar DOI resolution with dual-ended readout of a single unpolished LYSO crystal ($2 \times 2 \times 20 \text{ mm}^3$) using SiPMs.^{89,95}

A PET detector based on a 4×4 SiPM array coupled to a $13.2 \times 13.2 \times 10 \text{ mm}^3$ continuous LYSO crystal has been evaluated.⁸⁰ Using an original algorithm,⁴⁶ the entry point of the annihilation photon can be estimated to correct for the DOI. The FWHM of the detector spatial response yielded a resolution of 1.86 mm, with a very good uniformity with respect to the angle of incidence.

A multi-headed PET scanner has been proposed and simulated by Moehrs *et al.*^{30,55} Each detector head is composed of three stacks of detectors units, with each unit consisting of a SiPM array coupled to a continuous LSO slab of thickness 5 mm (Fig. 12b). The SiPM array is coupled to the crystal by a quartz light pipe (thickness 0–2 mm). The array has $1 \times 1 \text{ mm}^2$ SiPMs on a 1.5 mm pitch.⁴⁴ The depth of interaction information is given by the thickness of the

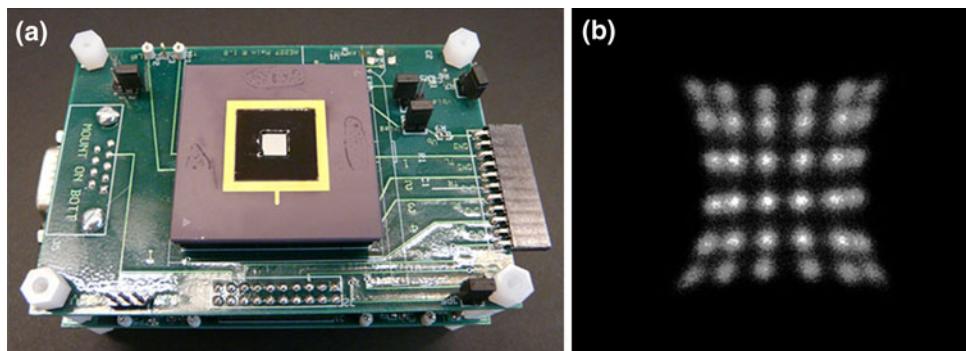


FIGURE 11. (a) $5 \times 5 \text{ mm}^2$ PS-SiPM (RMD Inc.). (b) Crystal map obtained with $5 \times 5 \text{ mm}^2$ PS-SiPMs coupled to a 6×6 array of $0.5 \times 0.5 \times 5 \text{ mm}^3$ LYSO crystals. All crystals can be easily resolved. McClish *et al.*⁵¹

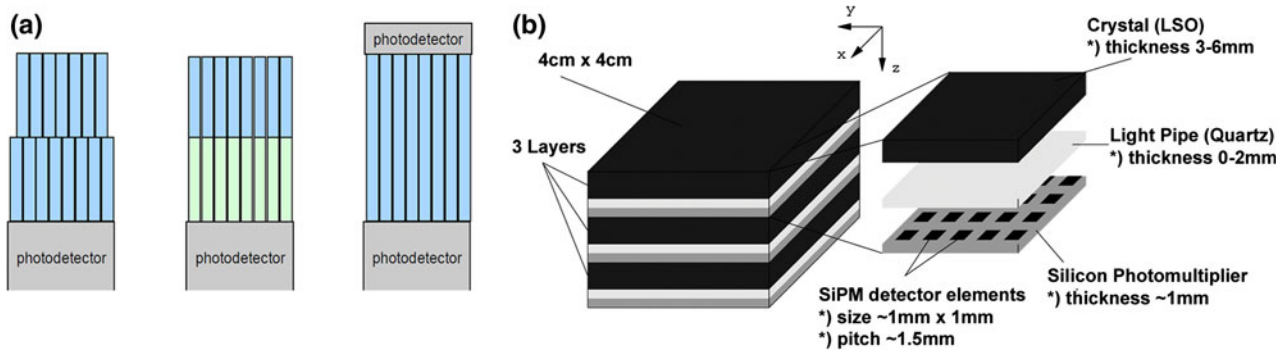


FIGURE 12. (a) DOI-encoding detectors. From left to right: offset crystal layers; different crystal layers; dual-ended readout. In each case, SiPM arrays could be utilized as the photodetector. (b) Prototype of a dual-head scanner with three module layers. Each layer is composed of a continuous LSO crystal coupled to a SiPM array. The thickness of the crystal defines the DOI resolution. Moehrs *et al.*⁵⁵

LSO slab and will be 5 mm. A simple prototype scanner would consist of two or four rotating $4 \times 4 \text{ cm}^2$ heads.

Time-of-Flight PET

In a PET scanner, an annihilation event is located on a line of response determined by the two detectors that detect the annihilation photons. With sufficient timing resolution, the location of the annihilation event along the line of response can be constrained to reduce the statistical noise.⁵⁸ This is known as time-of-flight PET. The position uncertainty along the line, Δx , as a function of the uncertainty in the timing measurement (the timing resolution), Δt , is given by

$$\Delta x = \frac{c}{2} \Delta t \quad (5)$$

where c is the speed of light. With good timing resolution (a few hundred of ps), the event can be located within a few cm along this line of response, thus providing higher signal-to-noise ratio images compared to images reconstructed using standard computed tomography algorithms with no timing information. This is equivalent to improving the effective sensitivity of the scanner by a factor inversely proportional to Δx .¹¹ For example, a timing resolution of 100 ps will constrain an annihilation event position to a Gaussian position distribution with a FWHM of 1.5 cm length along the line of response. The good intrinsic timing resolution of SiPMs along with potentially high photodetection efficiency, make SiPMs promising photodetectors for time-of-flight PET.

Coincidence timing resolutions between 0.7 and 4.5 ns have been routinely measured with coupling of LSO or LYSO crystals to SiPMs.^{42,43,50,61,66} Recently, a timing resolution as good as 240 ps was reported by Kim *et al.*³⁴ with LYSO crystals coupled to SiPMs with a high PDE of 45%. In general, improvements in PDE

should lead to improvements in timing resolution, as there will be less variability in the detection time of the first photoelectron, which determines the earliest time at which a signal can be sensed. Since the PDE depends on the overvoltage, the coincidence timing resolution depends strongly on the overvoltage. The timing resolution is only a weak function of the temperature. However, the overvoltage is temperature dependent, temperature still needs to be controlled. Just as with energy resolution, there is only a limited bias voltage range that provides the optimal timing resolution.³⁴ The variation of breakdown voltage from device to device creates challenges for detectors where a large number of SiPMs are tiled together, as the bias voltage may need to be separately adjusted to provide the overvoltage that gives the best timing resolution for each element.

Reasonable timing results have been obtained with SiPM arrays coupled to LSO or LYSO crystal arrays.^{36,45} One challenge posed by a multiplexed readout, such as a resistive network, is that the total dark count rate is higher, and parallel capacitance is increased, the latter slowing down the pulses and thus degrading the timing resolution.³⁴

LaBr₃ is a very attractive scintillator for time-of-flight PET due to its fast decay time and high light yield. Timing measurements with LaBr₃ coupled to SiPMs with an optimized geometry and light collection were reported by Schaart *et al.*⁸² The authors obtained an outstanding timing resolution of 101 ps FWHM with two LaBr₃/SiPM-based detectors in coincidence, and recently reported a timing resolution of 137 ps with LYSO crystals coupled to similar SiPMs.⁸¹

MRI-Compatible PET Detectors

When considering the development of integrated PET and MRI systems, several technical challenges become apparent. The goal is to provide a multimodal

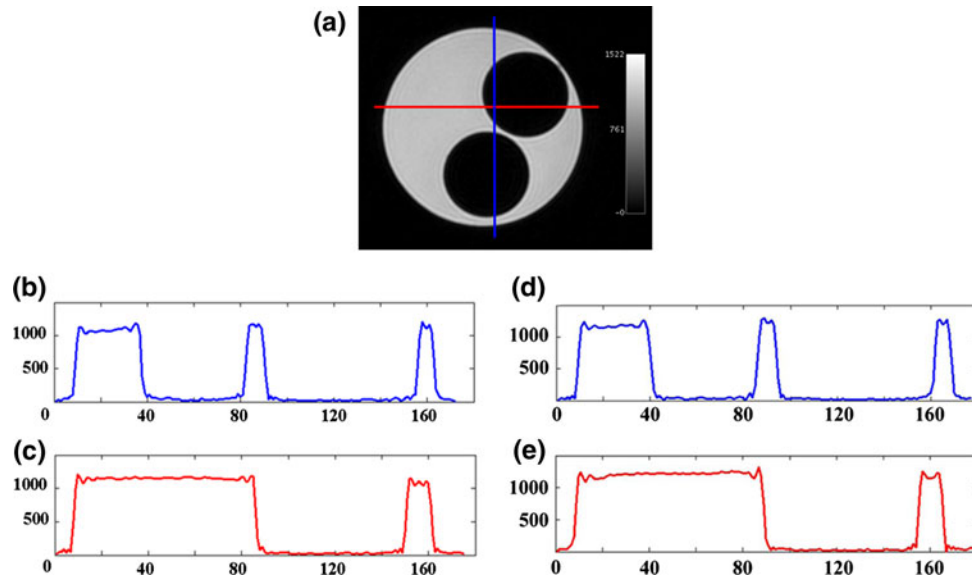


FIGURE 13. (a) MRI phantom images acquired with a gradient echo T2* sequence. Hong *et al.*³¹ In red: horizontal profile. In blue: vertical profile. (b) Vertical profile acquired without the PET detector. (c) Horizontal profile acquired without the PET detector. (d) Vertical profile acquired with the PET detector inside the bore. (e) Horizontal profile acquired with the PET detector inside the bore. Adapted from Hong *et al.*³¹ © 2008 IEEE.

system with optimal performance, without degradation due to the combination of the two technologies. Therefore, PET detectors should not create artifacts in MR images and PET signals should not be degraded by the presence of the MR system. PET detectors are sensitive to noise and may be affected by the presence of the magnetic field from the magnet, and the radiofrequency pulses and magnetic field gradient switching during MR sequences.⁴¹ In addition, eddy currents may be induced in the conducting structures of the detectors and the MR sequences can generate an increase of temperature that would modify the working point of the SiPMs. To the extent possible, non-magnetic materials should be used in the PET detectors to maintain the homogeneity of the magnetic field and not create susceptibility artifacts.¹⁶

SiPMs exhibit low sensitivity to magnetic fields due to the very high electric field in the narrow depletion region. The high gain should make them less sensitive to noise pickup. SiPMs-based PET detectors have been tested in whole-body clinical MRI systems (1.5 and 3 T) and no deterioration in energy spectrum and timing performance were observed when PET detectors were operated inside the magnet^{31,90} with MR sequences running. In MR images acquired with gradient echo T2* sequences, no artifacts appear to be caused by the SiPMs (Fig. 13). Similarly promising results have been achieved with SiPMs in higher field MR systems (7 T) designed for small-animal imaging.³⁶ A first prototype MR-compatible PET system, based on SiPM detectors, has recently been developed and successfully tested.¹⁰³

DISCUSSION

Are SiPMs Meeting Their Potential for Application in PET Imaging?

Energy resolutions of ~13% have been measured by different groups by coupling SiPMs to single LSO or LYSO crystals, at room temperature. That is comparable to measurements at 511 keV with single LSO crystals coupled to PMTs³ or APDs.^{33,69} Energy resolutions measured with SiPMs arrays coupled to pixelated crystals are slightly worse (19–25%) than some results obtained with large-area PS-APDs (16.2% at room temperature¹⁰⁵) but comparable to results obtained with LSO block detectors coupled to PMTs: For example energy resolutions of 15–25% were measured with 8×8 LSO arrays coupled to multichannel PMTs in microPET.¹⁷ In the case of SiPM arrays, there is a certain amount of light loss mainly due to the dead space between the pixels and better energy resolution can be expected with optimized light collection and continuous or tightly packed monolithic devices.

The feasibility of detectors based on scintillator arrays incorporating position-sensitive SiPMs has been demonstrated with good energy and timing resolution. Excellent timing resolution of better than 250 ps has been achieved.^{34,82} It appears in all respects that even these early generation SiPMs are extremely competitive with PMTs for readout of scintillators. Feasibility of a small-animal PET scanner based on SiPMs block detectors has been recently demonstrated with phantom and animal studies.^{38,103}

First tests of SiPM-based PET detectors in the presence of a magnetic field have revealed that the SiPM signals are not distorted by the MR system and that SiPM-based PET detectors do not generate artifacts in the MR images. These results confirm that silicon photomultipliers are well-suited for PET/MRI systems and may be considered for future generations of MR-compatible PET detectors.

What Improvements Can Be Expected and Which Challenges Are Posed?

Simple progress in light collection and thus in energy resolution can be made with arrays of SiPMs with enhanced packing fractions. Non-linearities in energy due to saturation effects could be either corrected or reduced by using a larger number of cells, thus improving the energy resolution. However, the number of cells will remain a limiting factor: assuming that the scintillator itself has perfect energy resolution, the energy resolution $\Delta E/E$ of a detector composed of such a scintillator coupled to a SiPM with m cells would be limited to:⁹⁴

$$\frac{\Delta E}{E} = \frac{2.92}{\sqrt{m}} \quad (6)$$

With LSO and LYSO, the scintillator itself (both due to light output, and non-linearities in light production) remains the dominant factor in the measured energy resolution, as evidenced by the fact SiPMs already achieve comparable energy resolution with these scintillators coupled to PMTs. However, it is conceivable that with a very bright scintillator, the number of cells would be a limiting factor, and that the energy resolution achieved with SiPMs would not be as good as with PMTs.

One possible performance limitation, illustrated by several studies,^{34,82,101} is that SiPMs show a longer rise time than PMTs. The rise time for SiPMs coupled to LYSO or LSO crystals is typically 15–20 ns whereas rise times of 0.7–5 ns can be measured with PMTs coupled to similar crystals. A major contribution to timing resolution is the time jitter due to electronic noise (σ_e). This time jitter σ_t is inversely proportional to the slope of leading edge (dV/dt) of the pulse when it crosses the leading edge discriminator threshold:¹⁰²

$$\sigma_t = \sigma_e \times \left(\frac{dV}{dt} \right)^{-1} \quad (7)$$

This formula shows that the greater the slope, the lower the time jitter σ_t , and thus indicates that a longer rise time might degrade the timing resolution. However, better timing resolution is obtained when triggering on the first detected photon from a light pulse

generated by a gamma-ray interaction in the scintillator.¹⁰⁰ Therefore, increasing the probability that the first photons produced will create a photoelectron by making devices with higher PDE will improve the timing resolution and may compensate for the slower rise time. The excellent timing resolution already achieved with carefully optimized SiPM and scintillator assemblies⁸² shows that this is not a major limitation of these devices. Timing may also be improved by active quenching techniques.⁹⁹

Overall, the challenge in SiPM development is to increase the active area while at least maintaining or preferably improving the performance. This is not trivial given considerations regarding increasing dark noise, the need to maintain high fill factors, the need to integrate ancillary circuits and functions to control large numbers of tightly packed SiPM pixels in array structures, and the likelihood of decreasing yields (and therefore increasing costs) as devices get larger and incorporate more SiPM pixels.

Integrated features such as pixel conditioning level or quenching circuits may improve the performance of SiPM in terms of pixel gain uniformity and timing. Advances in manufacturing should allow the production of larger-area devices, with better yield and consequently lower cost. Fully digital SiPMs that output digital signals will be well-suited to large-scale integration in PET scanners, although power consumption and heat dissipation issues may not be trivial in a scanner with tens of thousands of tightly packed detector elements.

CONCLUSION

With extremely promising published data demonstrating good energy and timing resolution, and the ability to decode arrays of scintillator elements, SiPMs have confirmed their potential as possible replacements for PMTs in PET detectors. One key question will largely determine whether PET scanners of the future will be based on SiPMs, and that is: Can SiPMs arrays or position-sensitive SiPMs be made with sensitive areas of at least $20 \times 20 \text{ mm}^2$ without any degradation in performance and at a cost per unit area significantly less than PMT's? If the answer is yes, then it would be hard to imagine that we will not see widespread adoption of SiPM technology in PET in the future.

ACKNOWLEDGMENTS

Some of the results presented in this review were supported by funding from NIH grant R01 CA134632. The authors thank Kanai Shah, Mickel McClish, and

Purushottam Dokhale at RMD Inc. (Watertown, MA) and Yongfeng Yang, Yibao Wu, Jeffrey Schmall, Julien Bec, and Sara St. James from UC Davis for useful discussions. The authors also thank the reviewers of this manuscript for their careful reading and extremely helpful suggestions.

OPEN ACCESS

This article is distributed under the terms of the Creative Commons Attribution Noncommercial License which permits any noncommercial use, distribution, and reproduction in any medium, provided the original author(s) and source are credited.

REFERENCES

- ¹Amplification Technologies. <http://www.amplificationtechnologies.com/>.
- ²Anfimov, N., I. Chirikov-Zorin, A. Dovlatov, O. Gavrishchuk, A. Guskov, N. Khovanskiy, Z. Krumshtein, R. Leitner, G. Meshcheryakov, A. Nagaytsev, A. Olchevski, T. Rezinko, A. Sadovskiy, Z. Sadygov, I. Savin, V. Tchalyshv, I. Tyapkin, G. Yarygin, and F. Zerrouk. Novel micropixel avalanche photodiodes (MAPD) with super high pixel density. *Nucl. Instrum. Methods Phys. Res. A*, 2010. doi:10.1016/j.nima.2010.07.003.
- ³Balcerzyk, M., M. Moszynski, M. Kapusta, D. Wolski, J. Pawelke, and C. L. Melcher. YSO, LSO, GSO and LGSO. A study of energy resolution and nonproportionality. *IEEE Trans. Nucl. Sci.* 47:1319–1323, 2000.
- ⁴Bar-Shalom, R., N. Yefremov, L. Guralnik, D. Gaitini, A. Frenkel, A. Kuten, H. Altman, Z. Keidar, and O. Israel. Clinical performance of PET/CT in evaluation of cancer: additional value for diagnostic imaging and patient management. *J. Nucl. Med.* 44:1200–1209, 2003.
- ⁵Bergeron, M., J. Cadorette, J.-F. Beaudoin, M. D. Lepage, G. Robert, V. Selivanov, M.-A. Tetrault, N. Viscogliosi, J. P. Norenberg, R. Fontaine, and R. Lecomte. Performance evaluation of the LabPET APD-based digital PET scanner. *IEEE Trans. Nucl. Sci.* 56:10–16, 2009.
- ⁶Beyer, T., D. W. Townsend, T. Brun, P. E. Kinahan, M. Charron, R. Roddy, J. Jerin, J. Young, L. Byars, and R. Nutt. A combined PET/CT scanner for clinical oncology. *J. Nucl. Med.* 41:1369–1379, 2000.
- ⁷Bondarenko, G., P. Buzhan, B. Dolgoshein, V. Golovin, E. Guschin, A. Ilyin, V. Kaplin, A. Karakash, R. Klanner, V. Pokachalov, E. Popova, and K. Smirnov. Limited Geiger-mode microcell silicon photodiode: new results. *Nucl. Instrum. Methods Phys. Res. A* 442:187–192, 2000.
- ⁸Bondarenko, G., B. Dolgoshein, V. Golovin, A. Ilyin, R. Klanner, and E. Popova. Limited Geiger-mode silicon photodiode with very high gain. *Nucl. Phys. B Proc. Suppl.* 61B:347–352, 1998.
- ⁹Brown, R. G. W., R. Jones, J. G. Rarity, and K. D. Ridley. Characterization of silicon avalanche photodiodes for photon-correlation measurements. 2. Active quenching. *Appl. Opt.* 26:2383–2389, 1987.
- ¹⁰Brown, R. G. W., K. D. Ridley, and J. G. Rarity. Characterization of silicon avalanche photodiodes for photon-correlation measurements. 1. Passive quenching. *Appl. Opt.* 25:4122–4126, 1986.
- ¹¹Budinger, T. F. Time-of-flight positron emission tomography: status relative to conventional PET. *J. Nucl. Med.* 24:73–78, 1983.
- ¹²Burnham, C. A., and G. L. Brownell. A multi-crystal positron camera. *IEEE Trans. Nucl. Sci.* 19:201–205, 1972.
- ¹³Buzhan, P., B. Dolgoshein, L. Filatov, A. Ilyin, V. Kantzerov, V. Kaplin, A. Karakash, F. Kayumov, S. Klemin, E. Popova, and S. Smirnov. Silicon photomultiplier and its possible applications. *Nucl. Instrum. Methods Phys. Res. A* 504:48–52, 2003.
- ¹⁴Buzhan, P., B. Dolgoshein, L. Filatov, A. Ilyin, V. Kaplin, A. Karakash, S. Klemin, R. Mirzoyan, A. N. Otte, E. Popova, V. Sosnovtsev, and M. Teshima. Large area silicon photomultipliers: performance and applications. *Nucl. Instrum. Methods Phys. Res. A* 567:78–82, 2006.
- ¹⁵Buzhan, P., B. Dolgoshein, A. Ilyin, V. Kantzerov, V. Kaplin, A. Karakash, A. Pleshko, E. Popova, S. Smirnov, Yu. Volkov, L. Filatov, S. Klemin, and F. Kayumov. An advanced study of silicon photomultiplier. In: Proceedings of Seventh International Conference on Advance Technology & Particle Physics, 2002, pp. 717–728.
- ¹⁶Catana, C., D. Procissi, Y. Wu, M. S. Judenhofer, J. Qi, B. J. Pichler, R. E. Jacobs, and S. R. Cherry. Simultaneous in vivo positron emission tomography and magnetic resonance imaging. *Proc. Natl. Acad. Sci. U.S.A.* 105:3705–3710, 2008.
- ¹⁷Cherry, S. R., Y. Shao, R. W. Silverman, K. Meadors, S. Siegel, A. Chatzioannou, J. W. Young, W. Jones, J. C. Moyers, D. Newport, A. Boutefnouchet, T. H. Farquhar, M. Andreaco, M. J. Paulus, D. M. Binkley, R. Nutt, and M. E. Phelps. MicroPET: a high resolution PET scanner for imaging small animals. *IEEE Trans. Nucl. Sci.* 44:1161–1166, 1997.
- ¹⁸Christian, J. F., C. J. Stapels, E. B. Johnson, M. McClish, P. Dokhale, K. S. Shah, S. Mukhopadhyay, E. Chapman, and F. L. Augustine. Advances in CMOS solid-state photomultipliers for scintillation detector applications. *Nucl. Instrum. Methods Phys. Res. A*, 2010. doi:10.1016/j.nima.2010.03.004.
- ¹⁹Corsi, F., M. Foresta, C. Marzocca, G. Matarrese, and A. Del Guerra. Basic: an 8-channel front-end ASIC for silicon photomultiplier detectors. *IEEE Nucl. Sci. Symp. Conf. Rec.* 1082–1087, 2009.
- ²⁰CPTA. Center of perspective technology and apparatus.
- ²¹Di Carli, M. F., S. Dorbala, J. Meserve, G. El Fakhri, A. Sitek, and S. C. Moore. Clinical myocardial perfusion PET/CT. *J. Nucl. Med.* 48:783–793, 2007.
- ²²Dolgoshein, B. Silicon photomultipliers in particle physics: possibilities and limitations. *Nucl. Instrum. Methods Phys. Res. A* 522:147–162, 2004.
- ²³Dolgoshein, B., V. Balagura, P. Buzhan, M. Danilov, L. Filatov, E. Garutti, M. Groll, A. Ilyin, V. Kantserov, V. Kaplin, A. Karakash, F. Kayumov, S. Klemin, V. Korbel, H. Meyer, R. Mizuk, V. Morgunov, E. Novikov, P. Pakhlov, E. Popova, V. Rusinov, F. Sefkow, E. Tarkovsky, and I. Tikhomirov. Status report on silicon photomultiplier development and its applications. *Nucl. Instrum. Methods Phys. Res. A* 563:368–376, 2006.
- ²⁴Finocchiaro, P., A. Pappalardo, L. Cosentino, M. Belluso, S. Billotta, G. Bonanno, B. Carbone, G. Condorelli, S. Di Mauro, G. Fallica, M. Mazzillo, A. Piazza, D. Sanfilippo, and G. Valvo. Characterization of a novel 100-channel silicon photomultiplier—part II: charge and time. *IEEE Trans. Electron Devices* 55:2765–2773, 2008.

- ²⁵Frach, T., and K. Fiedler. Digital silicon photomultiplier for TOF-PET. Patent No. US7723694, 2010.
- ²⁶Golovin, V. Avalanche photodetector. Patent No. RU 2142175, 1998.
- ²⁷Gomi, S., H. Hano, T. Iijima, S. Itoh, K. Kawagoe, S. H. Kim, T. Kubota, T. Maeda, T. Matsumura, Y. Mazuka, K. Miyabayashi, H. Miyata, T. Murakami, T. Nakadaira, T. Nakaya, H. Otono, E. Sano, T. Shinkawa, Y. Sudo, T. Takeshita, M. Taguchi, T. Tsubokawa, S. Uozumi, M. Yamaoka, H. Yamazaki, M. Yokoyama, K. Yoshimura, and T. Yoshioka. Development and study of the multi pixel photon counter. *Nucl. Instrum. Methods Phys. Res. A* 581: 427–432, 2007.
- ²⁸Hamamatsu Photonics K.K. <http://sales.hamamatsu.com>.
- ²⁹Hawkes, R., A. Lucas, J. Stevick, G. Llosa, S. Marcatili, C. Piemonte, A. D. Guerra, and T. A. Carpenter. Silicon photomultiplier performance tests in magnetic resonance pulsed fields. *IEEE Nucl. Sci. Symp. Conf. Rec.* 3400–3403, 2007.
- ³⁰Herbert, D. J., S. Moehrs, N. D'ascenzo, N. Belcari, A. Del Guerra, F. Morsani, and V. Saveliev. The silicon photomultiplier for application to high-resolution positron emission tomography. *Nucl. Instrum. Methods Phys. Res. A* 573:84–87, 2007.
- ³¹Hong, S. J., I. C. Song, M. Ito, S. I. Kwon, G. S. Lee, K.-S. Sim, K. S. Park, J. T. Rhee, and J. S. Lee. An investigation into the use of Geiger-mode solid-state photomultipliers for simultaneous PET and MRI acquisition. *IEEE Trans. Nucl. Sci.* 55:882–888, 2008.
- ³²Jackson, J. C., D. Phelan, A. P. Morrison, R. M. Redfern, and A. Mathewson. Toward integrated single-photon-counting microarrays. *Opt. Eng.* 42:112–118, 2003.
- ³³Kapusta, M., P. Crespo, D. Wolski, M. Moszynski, and W. Enghardt. Hamamatsu S8550 APD arrays for high-resolution scintillator matrices readout. *Nucl. Instrum. Methods Phys. Res. A* 504:139–142, 2003.
- ³⁴Kim, C. L., G.-C. Wang, and S. Dolinsky. Multi-pixel photon counters for TOF PET detector and its challenges. *IEEE Trans. Nucl. Sci.* 56:2580–2585, 2009.
- ³⁵Knoll, G. F. *Radiation Detection and Measurement* (3rd ed.). New York: Wiley, p. 816, 2000.
- ³⁶Kolb, A., E. Lorenz, M. S. Judenhofer, D. Renker, K. Lankes, and B. J. Pichler. Evaluation of Geiger-mode APDs for PET block detector designs. *Phys. Med. Biol.* 55:1815–1832, 2010.
- ³⁷Kuhn, A., S. Surti, J. S. Karp, G. Muehllehner, F. M. Newcomer, and R. Vanberg. Performance assessment of pixelated LaBr₃ detector modules for time-of-flight PET. *IEEE Trans. Nucl. Sci.* 53:1090–1095, 2006.
- ³⁸Kwon, S. I., J. S. Lee, H. S. Yoon, M. Ito, G. B. Ko, J. Y. Choi, S.-H. Lee, I. C. Song, J. M. Jeong, D. S. Lee, and S. J. Hong. Development of small animal PET prototype using a Geiger-mode APD: initial results of phantom and animal imaging studies (submitted).
- ³⁹Lacaita, A. L., F. Zappa, S. Bigliardi, and M. Manfredi. On the bremsstrahlung origin of hot-carrier-induced photons in silicon devices. *IEEE Trans. Electron Devices* 40:577–582, 1993.
- ⁴⁰Lecomte, R., J. Cadorette, S. Rodrigue, D. Lapointe, D. Rouleau, M. Bentourkia, R. Yao, and P. Msaki. Initial results from the Sherbrooke avalanche photodiode positron tomograph. *IEEE Trans. Nucl. Sci.* 43:1952–1957, 1996.
- ⁴¹Lee, J., and S. Hong. Geiger-mode avalanche photodiodes for PET/MRI. In: *Electronics for Radiation Detection*, edited by K. Iniewski. Boca Raton, FL: CRC Press, 2010, pp. 179–200.
- ⁴²Lee, J. S., M. Ito, K. S. Sim, B. Hong, K. S. Lee, J. Muhammad, J. T. Rhee, G. S. Lee, K. S. Park, I. C. Song, and S. J. Hong. Investigation of solid-state photomultipliers for positron emission tomography scanners. *J. Korean Phys. Soc.* 50:1332–1339, 2007.
- ⁴³Lee, C., Y. Soo Kim, W. Suk Sul, H. Kim, S. Han Shin, and G. Cho. Feasibility study on TOF-PET with fill factor improved SiPMs. *Nucl. Instrum. Methods Phys. Res. A*, 2010. doi:10.1016/j.nima.2010.06.155.
- ⁴⁴Llosá, G., R. Battiston, N. Belcari, M. Boscardin, G. Collazuol, F. Corsi, G.-F. D. Betta, A. D. Guerra, N. Dinu, G. Levi, S. Marcatili, S. Moehrs, C. Marzocca, and C. Piemonte. Novel silicon photomultipliers for PET applications. *IEEE Trans. Nucl. Sci.* 55:877–881, 2008.
- ⁴⁵Llosá, G., N. Belcari, M. G. Bisogni, G. Collazuol, S. Marcatili, P. Barrillon, C. De La Taille, S. Bondil-Blin, N. Dinu, M. Melchiorri, A. Tarolli, C. Piemonte, and A. Del Guerra. Energy, timing and position resolution studies with 16-pixel silicon photomultiplier matrices for small animal PET. *IEEE Trans. Nucl. Sci.* 56:2586–2593, 2009.
- ⁴⁶Maas, M. C., D. R. Schaart, D. J. J. Van Der Laan, P. Bruyndonckx, C. Lemaître, F. J. Beekman, and C. W. E. Van Eijk. Monolithic scintillator PET detectors with intrinsic depth-of-interaction correction. *Phys. Med. Biol.* 54:1893, 2009.
- ⁴⁷Maas, M. C., D. R. Schaart, D. J. J. Van Der Laan, H. T. Van Dam, J. Huijzen, J. C. Brouwer, P. Bruyndonckx, C. Lemaître, and C. W. E. Van Eijk. Signal to noise ratio of APD-based monolithic scintillator detectors for high resolution PET. *IEEE Trans. Nucl. Sci.* 55:842–852, 2008.
- ⁴⁸Mazzillo, M., G. Condorelli, A. Piazza, D. Sanfilippo, G. Valvo, B. Carbone, G. Fallica, S. Billotta, M. Belluso, G. Bonanno, A. Pappalardo, L. Cosentino, and P. Finocchiaro. Single-photon avalanche photodiodes with integrated quenching resistor. *Nucl. Instrum. Methods Phys. Res. A* 591:367–373, 2008.
- ⁴⁹Mazzillo, M., G. Condorelli, D. Sanfilippo, G. Valvo, B. Carbone, G. Fallica, S. Billotta, M. Belluso, G. Bonanno, L. Cosentino, and P. Finocchiaro. Silicon photomultiplier technology at STMicroelectronics. *IEEE Trans. Nucl. Sci.* 56:2434–2442, 2009.
- ⁵⁰Mcclish, M., P. Dokhale, J. Christian, E. Johnson, C. Stapels, R. Robertson, and K. S. Shah. Characterization of CMOS position sensitive solid-state photomultipliers. *Nucl. Instrum. Methods Phys. Res. A*, 2010. doi:10.1016/j.nima.2010.03.159.
- ⁵¹Mcclish, M., P. Dokhale, J. Christian, C. Stapels, E. Johnson, F. Augustine, and K. S. Shah. Performance measurements from LYSO scintillators coupled to a CMOS position sensitive SSPM detector. *Nucl. Instrum. Methods Phys. Res. A*, 2010. doi:10.1016/j.nima.2010.08.064.
- ⁵²Melcher, C. L., and J. S. Schweitzer. Cerium-doped lutetium oxyorthosilicate—a fast, efficient new scintillator. *IEEE Trans. Nucl. Sci.* 39:502–505, 1992.
- ⁵³Mirzoyan, R., M. Laatiaoui, and M. Teshima. Very high quantum efficiency PMTs with alkali photo-cathode. *Nucl. Instrum. Methods Phys. Res. A* 567:230–232, 2006.
- ⁵⁴Miyaoka, R. S., L. Xiaoli, C. Lockhart, and T. K. Lewellen. Comparison of detector intrinsic spatial resolution characteristics for sensor on the entrance surface and conventional readout designs. *IEEE Trans. Nucl. Sci.* 57:990–997, 2010.

- ⁵⁵Moehrs, S., A. Del Guerra, D. J. Herbert, and M. A. Mandelkern. A detector head design for small-animal PET with silicon photomultipliers (SiPM). *Phys. Med. Biol.* 51:1113, 2006.
- ⁵⁶Mosconi, L., W. H. Tsui, K. Herholz, A. Pupi, A. Drzezga, G. Lucignani, E. M. Reiman, V. Holthoff, E. Kalbe, S. Sorbi, J. Diehl-Schmid, R. Perneczky, F. Clerici, R. Caselli, B. Beuthien-Baumann, A. Kurz, S. Minoshima, and M. J. De Leon. Multicenter standardized ¹⁸F-FDG PET diagnosis of mild cognitive impairment, Alzheimer's disease, and other dementias. *J. Nucl. Med.* 49:390–398, 2008.
- ⁵⁷Moses, W. W. Trends in PET imaging. *Nucl. Instrum. Methods Phys. Res. A* 471:209–214, 2001.
- ⁵⁸Moses, W. W. Time of flight in PET revisited. *IEEE Trans. Nucl. Sci.* 50:1325–1330, 2003.
- ⁵⁹Moses, W. W., and S. E. Derenzo. Prospects for time-of-flight PET using LSO scintillator. *IEEE Trans. Nucl. Sci.* 46:474–478, 1999.
- ⁶⁰Mosset, J. B., O. Devroede, M. Krieguer, M. Rey, J. M. Vieira, J. H. Jung, C. Kuntner, M. Streun, K. Ziemons, E. Auffray, P. Sempere-Roldan, P. Lecoq, P. Bruyndonckx, J. F. Loude, S. Tavernier, and C. Morel. Development of an optimized LSO/LuYAP phoswich detector head for the Lausanne clearPET demonstrator. *IEEE Trans. Nucl. Sci.* 53:25–29, 2006.
- ⁶¹Musienko, Y., E. Auffray, A. Fedorov, M. Korzhi, P. Lecoq, S. Reucroft, and J. Swain. SSPM readout of LSO, (Lu-Y)AP:Ce and PWO-II pixels for PET detector modules. *IEEE Trans. Nucl. Sci.* 55:1352–1356, 2008.
- ⁶²Newman, R. Visible light from a silicon p–n junction. *Phys. Rev.* 100:700, 1955.
- ⁶³Ninkovic, J., L. Andricek, C. Jendrisyk, G. Liemann, G. Lutz, H.-G. Moser, R. Richter, and F. Schopper. The first measurements on SiPMs with bulk integrated quench resistors. *Nucl. Instrum. Methods Phys. Res. A*, 2010. doi:10.1016/j.nima.2010.07.012.
- ⁶⁴Nishikido, F., N. Inadama, I. Oda, K. Shibuya, E. Yoshida, T. Yamaya, K. Kitamura, and H. Murayama. Four-layer depth-of-interaction PET detector for high resolution PET using a multi-pixel S8550 avalanche photodiode. *Nucl. Instrum. Methods Phys. Res. A* 621:570–575, 2010.
- ⁶⁵Oldham, W. G., R. R. Samuelson, and P. Antognetti. Triggering phenomena in avalanche diodes. *IEEE Trans. Electron Devices* 19:1056–1060, 1972.
- ⁶⁶Otte, A. N., J. Barra, B. Dolgoshein, J. Hose, S. Klemin, E. Lorenz, R. Mirzoyan, E. Popova, and M. Teshima. A test of silicon photomultipliers as readout for PET. *Nucl. Instrum. Methods Phys. Res. A* 545:705–715, 2005.
- ⁶⁷Phelps, M. E., E. J. Hoffman, N. A. Mullani, and M. M. Ter-Pogossian. Application of annihilation coincidence detection to transaxial reconstruction tomography. *J. Nucl. Med.* 16:210–224, 1975.
- ⁶⁸Photonique SA. www.photonique.ch.
- ⁶⁹Pichler, B. J., B. K. Swann, J. Rochelle, R. E. Nutt, S. R. Cherry, and S. B. Siegel. Lutetium oxyorthosilicate block detector readout by avalanche photodiode arrays for high resolution animal PET. *Phys. Med. Biol.* 49:4305, 2004.
- ⁷⁰Piemonte, C. A new silicon photomultiplier structure for blue light detection. *Nucl. Instrum. Methods Phys. Res. A* 568:224–232, 2006.
- ⁷¹Piemonte, C., M. Boscardin, G.-F. D. Betta, M. Melchiorri, N. Zorzi, R. Battiston, A. D. Guerra, and G. Llosa. Recent developments on silicon photomultipliers produced at FBK-irst. *IEEE Nucl. Sci. Symp. Conf. Rec.* 2089–2092, 2007.
- ⁷²Ramilli, M. Characterization of SiPM: temperature dependencies. *IEEE Nucl. Sci. Symp. Med. Imaging Conf. Rec.* Oct 25–Oct 31, Dresden, Germany, 2008.
- ⁷³Rankowitz, S., J. S. Robertson, W. A. Higinbotham, and M. J. Rosenblum. Positron scanner for locating brain tumors. *IRE (Inst. Radio Engrs.) Intern. Con. Record* 9:49–56, 1961.
- ⁷⁴Renker, D. Geiger-mode avalanche photodiodes, history, properties and problems. *Nucl. Instrum. Methods Phys. Res. A* 567:48–56, 2006.
- ⁷⁵Ritzert, M., P. Fischer, V. Mlotok, I. Peri, C. Piemonte, N. Zorzi, V. Schulz, T. Solf, and A. Thon. Compact SiPM based detector module for time-of-flight PET/MR. Real Time Conference, 2009. RT '09. 16th IEEE-NPSS, 2009, pp. 163–166.
- ⁷⁶Sadygov, Z. Avalanche detector. Patent No. RU2102820, 1998.
- ⁷⁷Sadygov, Z., A. Olshevski, I. Chirikov, I. Zheleznykh, and A. Novikov. Three advanced designs of micro-pixel avalanche photodiodes: their present status, maximum possibilities and limitations. *Nucl. Instrum. Methods Phys. Res. A* 567:70–73, 2006.
- ⁷⁸Saoudi, A., C. M. Pepin, and R. Lecomte. Study of light collection in multi-crystal detectors. *IEEE Trans. Nucl. Sci.* 47:1634–1639, 2000.
- ⁷⁹Saveliev, V., and V. Golovin. Silicon avalanche photodiodes on the base of metal-resistor-semiconductor (MRS) structures. *Nucl. Instrum. Methods Phys. Res. A* 442:223–229, 2000.
- ⁸⁰Schaart, D. R., H. T. V. Dam, S. Seifert, R. Vinke, P. Dendooven, H. Löhner, and F. J. Beekman. A novel, SiPM-array-based, monolithic scintillator detector for PET. *Phys. Med. Biol.* 54:3501–3512, 2009.
- ⁸¹Schaart, D. R., S. Seifert, H. V. Dam, R. Vinke, P. Dendooven, H. Löhner, and F. J. Beekman. Progress in TOF-PET Scintillation Detectors Based on Silicon Photomultipliers. Kyoto, Japan: World Molecular Imaging Congress, 2010.
- ⁸²Schaart, D. R., S. Seifert, R. Vinke, H. T. V. Dam, P. Dendooven, H. Löhner, and F. J. Beekman. LaBr₃:Ce and SiPMs for time-of-flight PET: achieving 100 ps coincidence resolving time. *Phys. Med. Biol.* 55:179–189, 2010.
- ⁸³Seidel, J., J. J. Vaquero, S. Siegel, W. R. Gandler, and M. V. Green. Depth identification accuracy of a three layer phoswich PET detector module. *IEEE Trans. Nucl. Sci.* 46:485–490, 1999.
- ⁸⁴Sensl. <http://www.sensl.com/>.
- ⁸⁵Shah, K. S., R. Farrell, R. Grazioso, E. S. Harmon, and E. Karplus. Position-sensitive avalanche photodiodes for gamma-ray imaging. *IEEE Trans. Nucl. Sci.* 49:1687–1692, 2002.
- ⁸⁶Shah, K. S., R. Farrell, R. Grazioso, R. Myers, and L. Cirignano. Large-area APDs and monolithic APD arrays. *IEEE Trans. Nucl. Sci.* 48:2352–2356, 2001.
- ⁸⁷Shah, K. S., J. Glodo, M. Klugerman, W. W. Moses, S. E. Derenzo, and M. J. Weber. LaBr₃:Ce scintillators for gamma-ray spectroscopy. *IEEE Trans. Nucl. Sci.* 50:2410–2413, 2003.
- ⁸⁸Shao, Y., S. R. Cherry, K. Farahani, K. Meadors, S. Siegel, R. W. Silverman, and P. K. Marsden. Simultaneous PET and MR imaging. *Phys. Med. Biol.* 42:1965–1970, 1997.

- ⁸⁹Shao, Y., H. Li, and K. Gao. Initial experimental studies of using solid-state photomultiplier for PET applications. *Nucl. Instrum. Methods Phys. Res. A* 580:944–950, 2007.
- ⁹⁰Spanoudaki, V. C., A. B. Mann, A. N. Otte, I. Konorov, I. Torres-Espallardo, S. Paul, and S. I. Ziegler. Use of single photon counting detector arrays in combined PET/MR: characterization of LYSO-SiPM detector modules and comparison with a LSO-APD detector. *J. Instrum.* 2:12002, 2007.
- ⁹¹St James, S., Y. Yang, Y. Wu, R. Farrell, P. Dokhale, K. S. Shah, and S. R. Cherry. Experimental characterization and system simulations of depth of interaction PET detectors using 0.5 mm and 0.7 mm LSO arrays. *Phys. Med. Biol.* 54:4605, 2009.
- ⁹²Stewart, A. G., V. Saveliev, S. J. Bellis, D. J. Herbert, P. J. Hughes, and J. C. Jackson. Performance of 1-mm² silicon photomultiplier. *IEEE J. Quantum Electron.* 44:157–164, 2008.
- ⁹³STMicroelectronics. <http://www.st.com/stonline/>.
- ⁹⁴Stoykov, A., Y. Musienko, A. Kuznetsov, S. Reucroft, and J. Swain. On the limited amplitude resolution of multipixel Geiger-mode APDs. *J. Instrum.* 2:P06005, 2007.
- ⁹⁵Taghibakhsh, F., A. Reznik, and J. A. Rowlands. Silicon photomultipliers for positron emission tomography detectors with depth of interaction encoding capability. *Nucl. Instrum. Methods Phys. Res. A*, 2010. doi:10.1016/j.nima.2010.06.180.
- ⁹⁶Tai, Y.-C., A. Ruangma, D. Rowland, S. Siegel, D. F. Newport, P. L. Chow, and R. Laforest. Performance evaluation of the microPET focus: a third-generation microPET scanner dedicated to animal imaging. *J. Nucl. Med.* 46:455–463, 2005.
- ⁹⁷Tapfer, A., V. Spanoudaki, A. Mann, and S. I. Ziegler. Comparison of three approaches for timing optimization of a dual layer LSO-APD small animal PET scanner. In: W. C. 2009 IFBME Proceedings 25/II, edited by O. Dössel, and W. C. Schlegel. Munich: Springer Berlin Heidelberg, 2009, pp. 533–536.
- ⁹⁸Ter-Pogossian, M. M., M. E. Phelps, E. J. Hoffman, and N. A. Mullani. A positron-emission transaxial tomograph for nuclear imaging (PETT). *Radiology* 114:89–98, 1975.
- ⁹⁹Vasile, S., R. J. Wilson, S. Shera, D. Shamo, and M. R. Squillante. High gain avalanche photodiode arrays for direct applications. *IEEE Trans. Nucl. Sci.* 46:848–852, 1999.
- ¹⁰⁰Vinke, R., H. Löhner, D. R. Schaart, H. T. Van Dam, S. Seifert, F. J. Beekman, and P. Dendooven. Optimizing the timing resolution of SiPM sensors for use in TOF-PET detectors. *Nucl. Instrum. Methods Phys. Res. A* 610:188–191, 2009.
- ¹⁰¹Wang, G.-C. Timing optimization of solid-state photomultiplier based PET detectors. *IEEE Trans. Nucl. Sci.* 57:25–30, 2010.
- ¹⁰²Wilmschurst, T. H. Signal Recovery from Noise in Electronic Instrumentation. London: Hilger, p. 246, 1985.
- ¹⁰³Yamamoto, S., M. Imaizumi, T. Watabe, H. Watabe, Y. Kanai, E. Shimosegawa, and J. Hatazawa. Development of a Si-PM-based high-resolution PET system for small animals. *Phys. Med. Biol.* 55:5817, 2010.
- ¹⁰⁴Yang, Y., P. A. Dokhale, R. W. Silverman, K. S. Shah, M. A. Mcclish, R. Farrell, G. Entine, and S. R. Cherry. Depth of interaction resolution measurements for a high resolution PET detector using position sensitive avalanche photodiodes. *Phys. Med. Biol.* 51:2131–2142, 2006.
- ¹⁰⁵Yang, Y., Y. Wu, J. Qi, S. S. James, H. Du, P. A. Dokhale, K. S. Shah, R. Farrell, and S. R. Cherry. A prototype PET scanner with DOI-encoding detectors. *J. Nucl. Med.* 49:1132–1140, 2008.
- ¹⁰⁶Zecotek Photonics Inc. www.zecotek.com/.
- ¹⁰⁷Ziegler, S. I., B. J. Pichler, G. Boening, M. Rafecas, W. Pimpl, E. Lorenz, N. Schmitz, and M. Schwaiger. A prototype high-resolution animal positron tomograph with avalanche photodiode arrays and LSO crystals. *Eur. J. Nucl. Med. Mol. Imag.* 28:136–143, 2001.
- ¹⁰⁸Zorzi, N., M. Melchiorri, A. Piazza, C. Piemonte, and A. Tarolli. Development of large-area silicon photomultiplier detectors for PET applications at FBK. *Nucl. Instrum. Methods Phys. Res. A*, 2010. doi:10.1016/j.nima.2010.04.111.